High-pressure oxidation of ethane

Hashemi, Hamid; G. Jacobsen, Jon ; Rasmussen, Christian T. ; Christensen, Jakob Munkholt; Glarborg, Peter; Gersen, Sander; van Essen, Martijn; B. Levinsky, Howard ; Klippenstein, Stephen J.

Published in:
Combustion and Flame

Link to article, DOI:
10.1016/j.combustflame.2017.03.028

Publication date:
2017

Document Version
Peer reviewed version

High-Pressure Oxidation of Ethane

Hamid Hashemi*[a], Jon G. Jacobsen[a], Christian T. Rasmussen[a], Jakob M. Christensen[a], Peter Glarborg[a], Sander Gersen[b], Martijn van Essen[b], Howard B. Levinsky[b,c], Stephen J. Klippenstein[d]

[a]*DTU Chemical Engineering, Technical University of Denmark, DK-2800 Lyngby, Denmark*
[b]*DNV-GL Oil & Gas, 9704 CA Groningen, The Netherlands*
[c]*Energy & Sustainabiliy Research Institute, University of Groningen, Nijenborgh 4, 9747 AG Groningen, The Netherlands*
[d]*Chemical Sciences and Engineering Division, Argonne National Laboratory, Argonne, IL 60439, USA*

Abstract

Ethane oxidation at intermediate temperatures and high pressures has been investigated in both a laminar flow reactor and a rapid compression machine (RCM). The flow-reactor measurements at 600–900 K and 20–100 bar showed an onset temperature for oxidation of ethane between 700 K and 825 K, depending on pressure, stoichiometry, and residence time. Measured ignition delay times in the RCM at pressures of 10–80 bar and temperatures of 900–1025 K decreased with increasing pressure and/or temperature. A detailed chemical kinetic model was developed with particular attention to the peroxide chemistry. Rate constants for reactions on the $C_2H_5O_2$ potential energy surface were adopted from the recent theoretical work of Klippenstein. In the present work, the internal H-abstraction in CH_3CH_2OO to form CH_2CH_2OOH was treated in detail. Modeling predictions were in good agreement with data from the present work as well as results at elevated pressure from literature. The experimental results and the modeling predictions do not support occurrence of NTC behavior in ethane oxidation. Even at the high-pressure conditions of the present work where the $C_2H_5 + O_2$ reaction yields ethylperoxyl rather than $C_2H_4 + HO_2$, the chain branching sequence $CH_3CH_2OO \longrightarrow CH_2CH_2OOH \xrightarrow{+O_2} OOCH_2CH_2OOH \rightarrow$ *branching* is not competitive, because the internal H-atom transfer in CH_3CH_2OO to CH_2CH_2OOH is too slow compared to thermal dissociation to C_2H_4 and HO_2.

Keywords:

*Corresponding author. Fax: +45 4588 2258, URL: http://www.kt.dtu.dk, e-mail: hah@kt.dtu.dk (Hamid Hashemi)

1. Introduction

Investigation of ethane oxidation at high pressure and intermediate temperature is important from both fundamental and practical perspectives. From a practical point of view, ethane is the major non-methane component in natural gas, which is used in gas turbines and gas engines for power generation and transportation; variations in ethane fraction in natural gas may result in significant changes in the ignition properties of the fuel [1]. In addition, the use of ethane as an engine fuel is growing, in the first instance for ships transporting feedstock ethane. Knowledge of ethane oxidation is important for evaluating the potential of knock in the engines using these fuels, as well as for the development of HCCI engines [2] and assessing possible spontaneous ignition in lean-premixed gas turbines [3]. From a fundamental perspective, the oxidation of C_2H_6 plays an important role in the hierarchical structure of the reaction mechanisms of hydrocarbon fuels. To develop and verify these chemical kinetic models for hydrocarbon oxidation, measurements of the combustion characteristics at high pressure are essential.

While hydrocarbon ignition even at high temperatures relies on intermediate-temperature chemistry, this range of temperature, particularly at high pressure, has only been sparsely studied. Species concentrations have been reported from reactor experiments. Hunter et al. [4] studied ethane oxidation at temperatures of 915–966 K and pressures up to 10 atm in a flow reactor. A jet-stirred reactor was used by Dagaut et al. [5] to study ethane oxidation at temperatures of 800–1200 K and pressures of 1–10 atm. Tranter and co-authors [6–8] studied the pyrolysis and oxidation of ethane behind a reflected shock at pressures between 40 and 1000 bar over temperatures of 1000–1500 K by measuring major stable products using gas chromatography (GC).

A number of studies report the measurement of autoignition delay times for ethane [9–18]. Beerer and McDonell [17] evaluated the ignition delay of ethane and other lower alkanes in a flow reactor in the ranges of 785–935 K and of 7–15 atm. Shock tube studies by Lamoureux et al. [14], Aul et al. [16], and Zhang et al. [18] have characterized ignition delays for ethane in a wide range of temperature (1100–2700 K), pressure (1–21 bar), and equivalence ratio. Experiments performed by Gersen et al. [19] in a rapid compression

machine (RCM) at 930–1000 K and 20–40 bar extended the available data to higher pressure. However, these pressures are still below those relevant for modern internal combustion engines.

Chemical mechanisms for ethane oxidation have been developed by several groups [5, 20–22]. Two of the more recent models were developed specifically for high pressure application. Naik and Dean [21] suggested a model for the oxidation of ethane at high pressure and evaluated it against literature data. In a previous study from this laboratory [22], a kinetic model for the oxidation of the mixtures of CH_4 and C_2H_6 was established and evaluated against the results of high-pressure flow-reactor experiments of C_2H_6/CH_4 mixtures (C_2H_6/CH_4=13%, at maximum). Models developed for heavier hydrocarbons or components of natural gas (e.g., [23–26]) include by necessity subsets for ethane, but specific evaluation against ethane data has been limited.

To extend the available data toward conditions relevant to engines and gas turbines, this paper reports the results of ethane oxidation experiments in a laminar flow reactor at pressures of 20–100 bar and temperatures of 600–900 K under a wide range of stoichiometries. The data are supplemented by ignition delay times measured in a rapid compression machine (RCM) at temperatures of 900–1025 K and pressures of 10–80 bar under stoichiometric and fuel–lean ($\phi = 0.5$) conditions. A chemical kinetic model for ethane oxidation at increased pressure was established, based mostly on previous work [27]. The mechanism was updated with special emphasis on the peroxide chemistry. In particular, rate constants for reactions on the $C_2H_5O_2$ potential energy surface were adopted from the recent theoretical work of Klippenstein [28]. In the present work, the internal H-abstraction in CH_3CH_2OO to form CH_2CH_2OOH was studied at a high level of theory, allowing us to reevaluate the importance of the sequence

$$C_2H_5 \xrightarrow{+O_2} CH_3CH_2OO \longrightarrow CH_2CH_2OOH \xrightarrow{+O_2} OOCH_2CH_2OOH \rightarrow \text{branching}$$

for low temperature ethane oxidation. The kinetic model was evaluated by comparison to the present data as well as to data reported in literature.

2. Chemical kinetic model and ab initio calculations

A chemical kinetic model for ethane oxidation at increased pressure was established. The model, which is discussed in more detail below, was based on previous work on high-pressure oxidation of hydrogen [29], hydrogen/carbon monoxide [30], methane [22, 27], acetylene [31], ethylene [32], and methanol [33]. In the present work, it was updated with special emphasis on the peroxide chemistry and evaluated by comparison to the present data as well as to data reported in literature.

The key reaction in oxidation of ethane at intermediate temperature is $C_2H_5 + O_2$. This reaction, which involves multiple wells and multiple product channels, was recently studied by Klippenstein [28], along with other reactions on the $C_2H_5O_2$ potential energy surface, at a high level of theory. At the conditions of the present study (T > 600 K and high pressure), the reaction mainly proceeds by addition of molecular oxygen to the ethyl radical,

$$C_2H_5 + O_2(+M) \rightleftharpoons CH_3CH_2OO(+M) \qquad \text{(R12a)}$$

The fate of the ethylperoxy radical is important for the oxidation rate of ethane. Ethane is intermediate between the smallest alkane methane, which does not exhibit negative-temperature-coefficient (NTC) behavior and the larger alkanes such as propane and butane, which have distinct NTC behavior. As pointed out by Carstensen and Dean [34], experimental studies addressing the ignition of C_2H_6/O_2 mixtures appear to come to contradicting conclusions as to whether or not ethane oxidation shows NTC behavior. Knox and Norrish [35] reported distinct cool flame behavior for ethane while Dechaux and Delfosse [36] found no evidence of NTC behavior. In earlier studies, Townend and coworkers [37, 38] and Chirkov and Entelis [39] both observed a temperature range where the maximum rate of oxidation of ethane remained almost constant.

It is of interest whether the ethylperoxy radical participates in a chain-branching sequence similar to that of higher alkanes at temperatures below the NTC region. The initial steps are [40],

$$R + O_2 \rightleftharpoons ROO$$

$$\mathrm{ROO} \rightleftharpoons \mathrm{QOOH}$$

Once formed, QOOH may decompose to form the more reactive OH radical,

$$\mathrm{QOOH} \rightleftharpoons \mathrm{O-heterocycle} + \mathrm{OH}$$

or it may recombine with O_2, starting a chain-branching sequence,

$$\mathrm{QOOH} + \mathrm{O_2} \rightleftharpoons \mathrm{OOQOOH}$$

$$\mathrm{OOQOOH} \rightleftharpoons \mathrm{HOO\dot{Q}_{-H}OOH}$$

$$\mathrm{HOO\dot{Q}_{-H}OOH} \rightarrow \mathrm{\dot{O}Q_{-H}O} + \mathrm{OH} + \mathrm{OH}$$

In both cases the internal hydrogen abstraction reaction ROO $\rightleftharpoons$ QOOH, or for ethane,

$$\mathrm{CH_3CH_2OO}(+\mathrm{M}) \rightleftharpoons \mathrm{CH_2CH_2OOH}(+\mathrm{M}) \qquad \text{(R13a)}$$

may constitute a rate-limiting step. This reaction has previously been investigated theoretically [41–43] but only estimates of the high-pressure limit have been reported. In the present work we determine the rate constant for this step as a function of temperature and pressure, based on the potential energy surface (PES) and methods of Klippenstein [28].

2.1. Theory: CH_3CH_2OO isomerization

2.1.1. Methodology

The rovibrational properties of the stationary points on the PES were determined at the CCSD(T)/cc-pVTZ level. The B2PLYP-D3 double-hybrid density functional method [44, 45], with a cc-pVTZ basis set was employed in the mapping of the torsional modes. High level energy estimates were derived from estimates for (i) the CCSD(T) complete basis set (CBS) limit obtained from extrapolation of calculations for the aug′-cc-pVQZ and aug′-cc-pV5Z basis sets, (ii) higher order corrections from CCSDT(Q)/cc-pVDZ calculations, (iii) core-valence corrections from CCSD(T,full)/CBS calculations based on extrapolation of results for the cc-pcVTZ and cc-pcVQZ basis sets, (iv) rela-

tivistic corrections from CI/aug-cc-pcVTZ calculations, (v) diagonal Born-Oppenheimer corrections (DBOC) obtained at the HF/cc-pVTZ level, and (vi) anharmonic zero-point energy (ZPE) corrections calculated at the B3LYP/cc-pVTZ level.

The majority of the electronic structure calculations were performed with the MOLPRO software package of Werner and Knowles [46]. The CCSDT(Q) calculations were performed with the MRCC code of Kallay [47], while the DBOC were obtained with the CFOUR code of Stanton and Gauss [48]. The density functional theory calculations were performed with G09 [49].

The MESS code [50] was employed to obtain ab initio transition state theory based master equation (AI-TST-ME) predictions of the rate constants for this isomerization. This analysis includes a treatment of other channels on the PES as summarized in Ref. [28]. The collisional energy transfer rates were approximated as the product of Lennard-Jones collision rates with the exponential down model for the transition probability. For CH_3CH_2OO colliding with N_2, the Lennard-Jones parameters σ and ε were set to 3.95 Å and 286 cm^{-1}, respectively [51, 52]. The average downwards energy transferred, $< \Delta E_d >$, was set to 200 $(T/300)^{0.85}$ cm^{-1}.

2.1.2. Results

The zero-point corrected barrier height for the transition from CH_3CH_2OO to CH_2CH_2OOH is calculated to be 36.9 kcal mol^{-1}, while the 0 K reaction endothermicity is calculated to be 17.0 kcal mol^{-1}. This predicted barrier is just 0.1 kcal mol^{-1} lower than the G2-like value of 37.0 from Ref. [53]; the reaction endothermicities are also essentially identical.

An Arrhenius plot for the internal H-abstraction is shown in Fig. 1. Modified Arrhenius fits of the calculated rate constants are reported in Table 1. The upper bound in the temperature ranges for these fits are quite low, particularly for low pressures, due to the chemical instability of the CH_2CH_2OOH. Beyond that temperature CH_2CH_2OOH equilibrates with products more rapidly than it can be stabilized and should not be considered as a distinct chemical species.

2.2. Implications for the low-temperature oxidation of ethane.

The theoretical work by Klippenstein on reactions on the $C_2H_5O_2$ potential energy surface [28], including the internal H-abstraction in CH_3CH_2OO to form CH_2CH_2OOH dis-

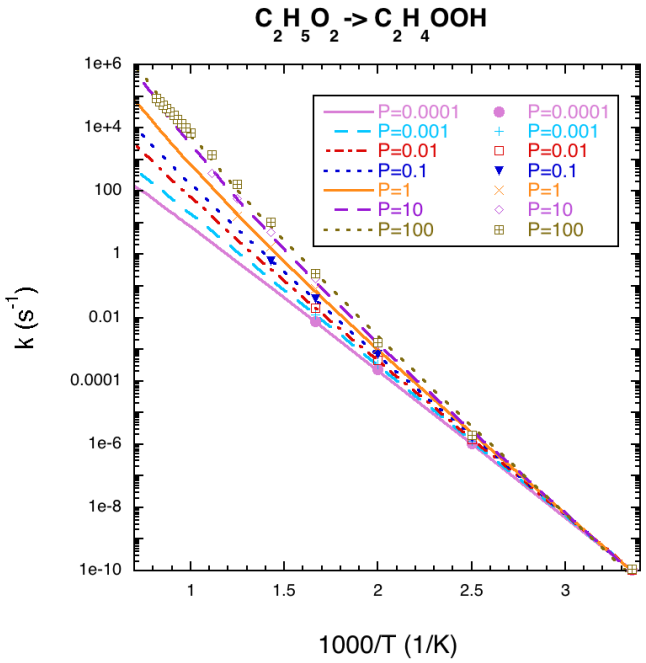

Figure 1: Plot of the temperature and pressure dependence of the rate coefficient for $CH_3CH_2OO \longrightarrow CH_2CH_2OOH$ (R13).

cussed above, allows us to reassess the importance of the sequence $C_2H_5 \xrightarrow{+O_2} CH_3CH_2OO \longrightarrow CH_2CH_2OOH \xrightarrow{+O_2} OOCH_2CH_2OOH \rightarrow$ branching (A). Figure 2 shows a simplified pathway diagram for conversion of CH_3CH_2OO under conditions representative of the present work, i.e., 500-900 K, 100 bar and an O_2 concentration in the percent range.

Under high-pressure conditions, the reaction of ethyl with O_2 almost solely leads to formation of ethylperoxy (R12a), with concerted elimination of HO_2 (R12b) becoming important only at higher temperatures or lower pressures. The figure shows that ethyl peroxy is mostly consumed by thermal dissociation to C_2H_4 and HO_2 (R13b), with only about 1% isomerizing to CH_2CH_2OOH (R13a). The CH_2CH_2OOH radical reacts rapidly with O_2 to form $OOCH_2CH_2OOH$, which can undergo internal H-abstraction and subsequently dissociate, forming two OH radicals.

Due to the low fraction of CH_3CH_2OO isomerizing to CH_2CH_2OOH, the amount of chain branching via sequence (A) is limited. This has the implication that we would not expect to observe NTC behavior in the oxidation of ethane in the present work. As the pressure is decreased, NTC behavior is even more unlikely since the major product channel for $C_2H_5 + O_2$ will shift from formation of ethylperoxy (R12a) to formation of $C_2H_4 + HO_2$ (R12b). This is in line with suggestions in the literature [34, 42, 54], based

Table 1: Modified Arrhenius fits of calculated rate constants for $CH_3CH_2OO \rightarrow CH_2CH_2OOH$.[a]

P[b]	A	n	E_a	T Range
0.0001	3.15E31	-8.25	29360	300-600
0.0003	3.50E30	-7.88	29330	300-600
0.001	1.52E29	-7.37	29210	300-600
0.003	3.47E27	-6.77	29000	300-600
0.01	3.57E25	-6.04	28780	300-600
0.03	1.60E24	-5.51	28800	300-700
0.1	1.44E21	-4.40	28410	300-700
0.3	2.85E19	-3.73	28490	300-700
1	1.27E17	-2.81	28500	300-800
3	5.27E14	-1.90	28470	300-900
10	4.67E13	-1.40	28970	300-900
30	4.21E12	-0.92	29380	300-1100
100	1.87E08	0.57	28590	300-1200

[a] $k = A\ T^n \exp(-E/(RT))$ with A in s^{-1}, E_a in cal mol^{-1}, and T in K.
[b] Pressure in atm

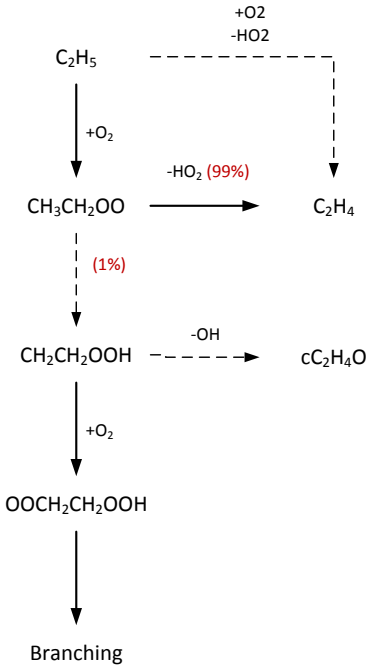

Figure 2: Simplified reaction path diagram for low-temperature, high-pressure oxidation of ethane, emphasizing the importance of NTC-type chemistry. The analysis is made for temperatures of 500-900 K, 100 bar, and 4% O_2.

on the higher calculated barrier for the 1,4 H-migration versus the concerted elimination for the formation of ethene and HO_2.

2.3. Reaction mechanism

In a previous study from this laboratory [22], a chemical kinetic model for combustion of CH_4 and C_2H_6 was proposed and evaluated against experimental data at high pressures for CH_4/C_2H_6 mixtures. In more recent work, the subsets describing oxidation of hydrogen as well as C_1 and C_2 hydrocarbons were updated [27, 29, 31]. In the present work, the reactions of the ethane subset were reviewed and more accurate rate constants were implemented where possible. Table 2 lists rate constants for selected species in the C_2 oxidation subset; the full mechanism is available in Supplemental Material.

Table 2: Selected reactions from ethane oxidation mechanism. The rate constants are in the form of $k = A\,T^n\,\exp\left(\frac{-E}{RT}\right)$. Units are *mol*, *cm*, *K*, *s*, and *cal*.

	Reaction	A	n	E	Note/Ref.
R1	$CH_3 + CH_3(+M) = C_2H_6(+M)$	9.5E14	-0.540	179	[55]
	Low-pressure limit:	1.3E41	-7.000	2762	
	Troe parameters:	0.62	73	1180	1.E30
R2	$C_2H_6 + H = C_2H_5 + H_2$	7.4E03	3.100	5340	[56]
	duplicate rate constant	3.3E14	0.000	13667	
R3	$C_2H_6 + O = C_2H_5 + OH$	1.8E05	2.800	5800	[57]
R4	$C_2H_6 + OH = C_2H_5 + H_2O$	1.6E06	2.220	741	[58]
R5	$C_2H_6 + HO_2 = C_2H_5 + H_2O_2$	8.7E04	2.650	18900	[34] [a]
R6	$C_2H_6 + O_2 = C_2H_5 + HO_2$	2.9E07	1.900	49548	[59]
R7	$C_2H_6 + CH_3 = C_2H_5 + CH_4$	3.5E01	3.440	10384	[60]
R8	$C_2H_4 + H(+M) = C_2H_5(+M)$	1.4E09	1.463	1355	[61]
	Low-pressure limit:	2.0E39	-6.642	5769	
	Troe parameters:	-0.569	299	9147	152.4
R9	$CH_3 + CH_3 = C_2H_5 + H$	5.4E13	0.000	16055	[57]
R10a	$C_2H_5 + OH = C_2H_4 + H_2O$	4.7E18	-1.581	7999	[62] [b]
R10b	$C_2H_5 + OH = CH_3 + CH_2OH$	6.5E22	-2.442	12647	[62] [b]
R11	$C_2H_5 + HCO = CH_3 + CH_2CHO$	6.5E22	-2.442	12647	[62] est [b]

Continued on next page

Table 2 – *continued from previous page*

		Arrhenius data			
R12a	$C_2H_5 + O_2$=CH_3CH_2OO	1.6E30	-5.560	5909	[28] [b]
R12b	$C_2H_5 + O_2$=$C_2H_4 + HO_2$	1.9E11	0.140	6373	[28] [b]
R12c	$C_2H_5 + O_2$=CH_2CH_2OOH	1.9E15	-1.720	8034	[28] [b]
R12d	$C_2H_5 + O_2$=$cC_2H_4O + OH$	9.7E14	-1.220	12500	[28] [b]
R13a	CH_3CH_2OO=CH_2CH_2OOH	1.9E08	0.570	28590	*p.w.* [b]
R13b	CH_3CH_2OO=$C_2H_4 + HO_2$	1.6E26	-4.370	34840	[28] [b]
R13c	CH_3CH_2OO=$cC_2H_4O + OH$	2.5E31	-6.100	44560	[28] [b]
R14	$CH_3CH_2OO + HO_2$=$CH_3CH_2OOH + O_2$	3.6E11	0.000	-1267	[63]
R15	CH_2CH_2OOH=$cC_2H_4O + OH$	3.2E21	-2.970	16400	[28] [b]
R16	CH_3CH_2OOH=$CH_3CH_2O + OH$	1.4E33	-5.270	48696	[64] [b]
R17	$CH_3CH_2O(+M)$=$CH_2O + CH_3(+M)$	6.3E10	0.930	17098	[65]
	Low-pressure limit:	4.7E25	0.930	16532	
	Troe parameters:	0.426	0.3 2278	100000	
R18a	$C_2H_4 + HO_2$=CH_2CH_2OOH	4.4E18	-2.170	16840	[28] [b]
R18b	$C_2H_4 + HO_2$=$cC_2H_4O + OH$	2.2E12	0.160	19980	[28] [b]

[a] see text.

[b] at 100 atm pressure. For other pressures see the mechanism file in the Supplemental Material.

The mechanism takes into account the prompt dissociation of the weakly bound radical HCO, based on the recent work of Labbe et al. [66]. Weakly bound free radicals have low dissociation thresholds, facilitating dissociation during the vibrational-rotational relaxation process at high temperatures where the timescales for dissociation and collisional relaxation become comparable. The prompt dissociation of HCO yields atomic hydrogen, promoting the radical pool. We adopt the method of Labbe et al. [66] to derive prompt dissociation fractions of important HCO-forming reactions.

The dissociation of ethane (R1(b)) can initiate pyrolysis/oxidation at high temperatures. At the temperatures of the flow reactor and RCM experiments, this reaction is

favored in the reverse direction where it acts as a chain-termination path,

$$CH_3 + CH_3(+M) \rightleftharpoons C_2H_6(+M) \quad \text{(R1)}$$

At the pressures of this study, the rate constant for reaction R1 approaches its high-pressure limit. We adopt the value of the high-pressure limit from the theoretical work of Klippenstein et al. [55]. Their calculation shows a slight negative temperature dependency, in line with most earlier measurements as well as the recent one by Sangwan et al. [67].

Ethane is mostly consumed by H-abstraction reactions with the radical pool, e.g.,

$$C_2H_6 + H \rightleftharpoons C_2H_5 + H_2 \quad \text{(R2)}$$

$$C_2H_6 + O \rightleftharpoons C_2H_5 + OH \quad \text{(R3)}$$

$$C_2H_6 + OH \rightleftharpoons C_2H_5 + H_2O \quad \text{(R4)}$$

$$C_2H_6 + HO_2 \rightleftharpoons C_2H_5 + H_2O_2 \quad \text{(R5)}$$

The H-abstraction by a hydrogen atom from ethane (R2) has a relatively high barrier ($\sim$5.1 kcal mol^{-1} [56]), so it is mostly favored at high temperatures. We rely on the results of Sivaramakrishnan et al. [56] who measured k_2 in a shock tube at 1128–1299 K and extrapolated the rate constant to 300–2000 K from theory and previous measurements. Their rate constant has a higher sensitivity to temperature than the recommendation by Baulch et al. [57]. The most important consumption step for ethane is typically reaction with OH (R4), partly due to its low barrier ($\sim$0.7 kcal mol^{-1} [58]) and partly due to the abundance of OH radicals over a fairly wide range of stoichiometry. The rate constant for reaction R4 is taken from Krasnoperov and Michael [58]; their value agrees well with earlier determinations.

Hydrogen-abstraction from ethane by HO_2 (R5) becomes increasingly important with decreasing temperature and increasing pressure. The only reliable experimental determination of k_5 was conducted by Baldwin et al. [68]. They measured $k_5/(k_{HO_2+HO_2})^{0.5}$ at four temperatures in the 673–773 K range. We have re-evaluated their values of k_5, using the recent rate constant for HO_2 + HO_2 from Zhou et al. [69]. The results are compared

with theoretical rate constants for C_2H_6 + HO_2 on Fig. 3. Carstensen and coworkers calculated k_5 both from estimation rules [34] and from CBS-QB3 ab initio calculations [34, 70]. More recently, Aguilera-Iparraguirre et al. [71] investigated reaction R5 at the CCSD(T) level but adjusted the results according to higher level benchmark calculations on CH_4 + HO_2.

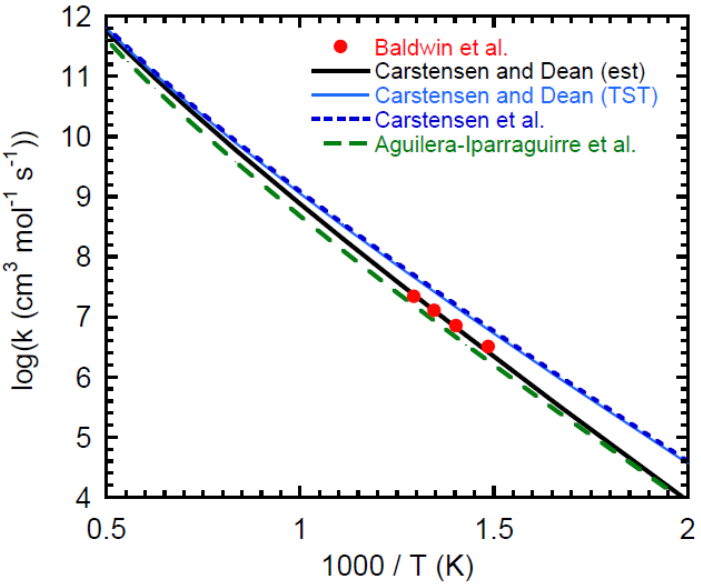

Figure 3: Arrhenius plot for the reaction $C_2H_6+HO_2 \rightleftharpoons C_2H_5+H_2O_2$. The symbols denote experimental values from Baldwin et al. [68], obtained as $k_5/(k_{HO_2+HO_2})^{0.5}$ and reinterpreted in the present work with an updated value of $k_{HO_2+HO_2}$ [69]. Lines denote calculated rate constants from Carstensen and Dean [34], Carstensen et al. [70], and Aguilera-Iparraguirre et al. [71]. The rate constant from Carstensen et al. [70] was divided by a factor of 10 to correct for a typo in the A-factor.

The theoretical rate constants for R5 vary up to a factor of four but agree with the measurements of Baldwin et al. roughly within a factor of two. We have adopted the value from Carstensen and Dean derived from estimation rules; this value is in between the theoretical rate constants and agrees closely with the data derived from Baldwin et al. Modeling predictions of high-pressure intermediate temperature ethane oxidation are sensitive to k_5 and the flow reactor data discussed below support the results from Baldwin et al.

The reaction between ethane and molecular oxygen,

$$C_2H_6 + O_2 \rightleftharpoons C_2H_5 + HO_2 \qquad \text{(R6)}$$

is an initiation step at intermediate temperatures. For this reaction, we rely on calcu-

lations by Sharipov and Starik [59] giving a rate constant around 40% lower (at 700 K) than the estimation of Baulch et al. [57].

The reaction between ethane and the methyl radical,

$$C_2H_6 + CH_3 \rightleftharpoons C_2H_5 + CH_4 \tag{R7}$$

can be important under reducing conditions. The rate constant is taken from the work of Peukert et al. [60] who combined shock-tube measurements at 1153–1297 K with TST calculations to obtain a rate constant valid in the 500–2000 K range.

At the present temperatures and pressure, the ethyl radical mainly adds to molecular oxygen,

$$C_2H_5 + O_2(+M) \rightleftharpoons CH_3CH_2OO(+M) \tag{R12a}$$

For the addition step, as well as for the other branches of the $C_2H_5 + O_2$ reaction (i.e., R12b, R12c, and R12d), we rely on the calculations by Klippenstein [28].

For the reaction of ethyl with hydroxyl radicals (R10a, R10b),

$$C_2H_5 + OH(+M) \rightleftharpoons C_2H_4 + H_2O(+M) \tag{R10a}$$

$$C_2H_5 + OH(+M) \rightleftharpoons CH_3 + CH_2OH(+M) \tag{R10b}$$

we adopt the rate constants obtained theoretically by Labbe et al. [62].

As discussed above, ethylperoxy radicals (CH_3CH_2OO) may isomerize internally to CH_2CH_2OOH or dissociate to either $C_2H_4 + HO_2$ or $cC_2H_4O + OH$ [28].

$$CH_3CH_2OO \rightleftharpoons CH_2CH_2OOH \tag{R13a}$$

$$CH_3CH_2OO \rightleftharpoons C_2H_4 + HO_2 \tag{R13b}$$

$$CH_2CH_2OOH \rightleftharpoons cC_2H_4O + OH \tag{R13c}$$

Alternatively, ethylperoxy can abstract hydrogen from stable molecules such as CH_4 and C_2H_6, or combine with other radicals. For the H-abstraction from CH_4 and C_2H_6, we adopted the rate constants from the theoretical work of Carstensen et al. [70]. In

the absence of measurements or theoretical determinations, H-abstraction from most other components are estimated by analogy to the reactions of CH_3OO and HO_2 (see Supplemental Material).

Hydrogen-abstraction by CH_3CH_2OO from stable molecules yields ethyl hydroperoxide (CH_3CH_2OOH). Ethyl hydroperoxide may react with radicals or dissociate thermally. The rate constant for decomposition of ethyl hydroperoxide is drawn from a theoretical determination by Chen et al. [64]. Only the channel to $CH_3CH_2O + OH$ (R16) is important under combustion conditions. For the radical reactions, we estimate the rate constant by analogy to CH_3OOH reactions.

The hydroxyalkyl radical CH_2CH_2OOH would be expected to recombine rapidly with O_2,

$$CH_2CH_2OOH + O_2(+M) \rightleftharpoons OOCH_2CH_2OOH(+M)$$

To assess the importance of the sequence $CH_2CH_2OOH \xrightarrow{+O_2} OOCH_2CH_2OOH \rightarrow$ branching, we conducted calculations including the overall reaction,

$$CH_2CH_2OOH + O_2 \rightarrow CH_2O + HCO + OH + OH$$

with a rate constant estimated to be similar to that of $C_2H_5 + O_2$ recombination. However, due to the small amounts of CH_2CH_2OOH formed by isomerization of CH_3CH_2OO (R13a), predictions were not sensitive to this step and this reaction pathway is not included in the final mechanism.

Ethene is an important intermediate under the current conditions. The reaction subset for ethene, discussed elsewhere [32], was adopted from recent work [27] without changes. Modeling predictions show sensitivity to the rate constant for the complex

reaction between ethene and the hydroxyl radical,

$$\begin{aligned} C_2H_4 + OH(+M) &\rightleftharpoons C_2H_3 + H_2O(+M) && \text{(R19a)} \\ &\rightleftharpoons CH_3 + CH_2O(+M) && \text{(R19b)} \\ &\rightleftharpoons CH_3CHO + H(+M) && \text{(R19c)} \\ &\rightleftharpoons CH_2CHOH + H(+M) && \text{(R19d)} \\ &\rightleftharpoons CH_2CH_2OH(+M) && \text{(R19e)} \end{aligned}$$

We adopt the rate coefficients from the theoretical work of Senosiain et al. [72]. The direct hydrogen abstraction to form vinyl radicals (C_2H_3) is the major channel at intermediate to high temperatures. More recently, Vasu et al. [73] measured the overall rate of the title reaction over 973–1438 K and pressures of 2–10 atm; conditions where formation of C_2H_3 is expected to be dominant. Their results indicate a rate constant for the C_2H_3 branch around 50 % higher (at 800 K) than Senosiain et al. [72], i.e., in agreement with the theoretical value within the uncertainty.

3. Experimental

3.1. The laminar flow reactor

The experimental setup was a laboratory-scale high-pressure laminar-flow reactor designed to approximate plug flow. The setup was described in detail elsewhere [30] and only a brief description is provided here. The system was used here for investigation of ethane oxidation chemistry at pressures from 20 to 100 bar, temperatures up to 900 K, and flow rates of $\sim$ 3 Nl min^{-1} (STP; 1 atm and 273.15 K).

The reactions took place in a tubular quartz reactor (inner diameter of 8 mm), enclosed in a stainless steel tube that acted as a pressure shell. Using a quartz tube and conducting experiments at high pressure minimized the contribution from heterogeneous reactions at the reactor wall. The steel tube was placed in a tube oven with three individually controlled electrical heating elements that produced an isothermal reaction zone in the middle of the reactor. A moving thermocouple was used to measure the temperature profile inside the pressure shell wall after stabilizing the system. The system was pressurized from the feed gas cylinders. The reactor pressure was monitored

upstream of the reactor by a differential pressure transducer and controlled by a pneumatic pressure valve positioned after the reactor. The pressure fluctuations were less than 0.2 % during the experiments. The reactant gases were premixed before entering the reactor. All gases used in the present experiments were high purity gases or mixtures with certified concentrations (±2% uncertainty). Downstream of the reactor, the system pressure was reduced to atmospheric level prior to product analysis, which was conducted by an on-line *6890N Agilent Gas Chromatograph* (GC-TCD/FID from Agilent Technologies). All GC sampling and measurements were repeated at least twice to reduce measurement uncertainties. Distinguishing methanol from acetaldehyde was not possible due to signal overlapping in the GC. The signal areas corresponding to the sum of these components were measured and quantified by using the response factor of methanol, but the reported quantity was less accurate especially when a considerable acetaldehyde yield was expected. A general uncertainty of 6% is estimated for measurements by GC.

The plug flow assumption was shown by Rasmussen et al. [30] to be a good approximation for the present operating conditions. Figure 4 shows the measured temperature profiles for different isotherms while the flow was pure nitrogen. It was found that use of the full temperature profiles promoted the accuracy of simulations. Therefore, a plug flow model with constrained temperature and pressure was used for simulations in Chemkin [74]. Temperature profiles measured at different pressures revealed sensitivity of temperature profiles to the system pressure, most likely due to fluctuations in nitrogen supply of the pressure shell at higher pressures. Therefore separate temperature profiles for each pressure are provided as supplementary material. The uncertainty in the gas temperature due to heat release of reactions was limited by a high level of dilution. Simulations in Chemkin [74] with a constant pressure and enthalpy (adiabatic) model lead to a maximum 22 K temperature rise. However, because of the fast heat transfer from hot gases to the pressure shell, especially in such a narrow reactor, the deviation of the gas temperature from the measured temperature should be even smaller.

3.2. The rapid compression machine (RCM)

The experiments were conducted in a Rapid Compression Machine (RCM), described in detail previously [19, 75], of the same design, construction and specification as reported

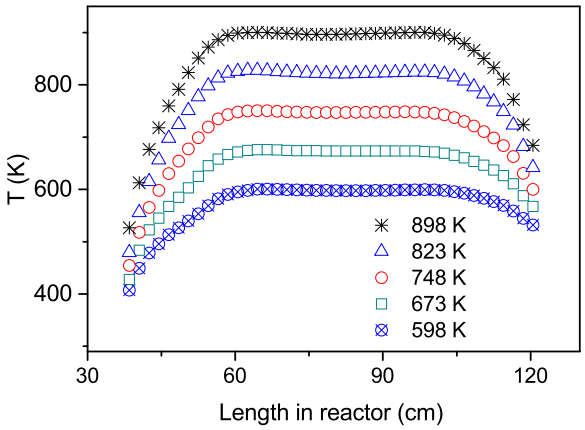

Figure 4: Measured temperature profiles across the reaction zone. The flow rate was ∼3 NL min^{-1} at a pressure of 30 bar. The isothermal zone shrunk slightly at higher pressures.

in [76, 77]. A recommended creviced piston head [78], designed for this machine, was used in order to preserve a homogeneous reacting core. The gas mixtures were compressed in 10–20 ms to peak pressures that indicate the end of the compression, wherein the majority of the pressure rise took place in less than 3 ms. The dynamic pressures during compression and throughout the post compression period were measured using a Kistler quartz pressure sensor with thermo-shock optimized construction. Autoignition delay times for the $C_2H_6/O_2/Ar/N_2$ mixtures were obtained in a range of temperatures (900–1025 K) and pressures (10–80 bar) at ϕ=1.0 and ϕ=0.5. The composition of the studied gas mixtures, expressed in mole percent are given in Table 3. The total concentration of diluting inert gases were close to that of nitrogen in air, while the Ar/N_2 ratio was chosen to provide the temperature range studied after compression for all fuels.

Table 3: Composition of gas mixtures investigated in the RCM, expressed in mole %.

Mixture	C_2H_6	O_2	N_2	AR	Φ
A	5.4	18.9	30	45.7	1
B	2.8	19.6	30	47.6	0.5

The gas mixtures were prepared in advance in a 10 litre gas bottle and allowed to mix for 72 hours to ensure homogeneity. All test gases used in the experiments had purity greater than 99.9%. The desired gas temperature at the end of compression of the mixtures was obtained by changing the stroke length while the pressure at the end

of compression was changed by varying the initial pressure. To avoid the difficulty of calculating an effective compression ratio based on the unknown volume of the core gas within the combustion chamber, the ratio of measured pressures (P_c, P_i) was used to calculate the temperature (T_c) of the adiabatic core gas using the following equation,

$$\int_{T_i}^{T_c} \frac{\gamma}{\gamma - 1} \frac{dT}{T} = ln \frac{P_c}{P_i} \tag{1}$$

Here, $\gamma = C_p(T)/C_v(T)$. The heat capacities used in the calculation were expressed as temperature dependent polynomials [19]. The uncertainty of the calculated core gas temperatures (T_c) was less than ± 3.5 K for all measurements. The reproducibility of the measured ignition delay times under identical conditions was better than $\sim$5% and the uncertainty in deriving the ignition delay from the measurements was $\sim$ 0.3 ms.

Since RCM experiments involve compression and heat losses it is necessary to account for these effects in performing the numerical simulations. In this study compression and heat loss are taken into account in the model by specifying the specific volume of the adiabatic core as input into the simulations [76, 79, 80] which are performed with the SENKIN code [81] of the CHEMKIN II suite [82]. Since no multistage ignition phenomena were observed in the experiments, the specific volume of the adiabatic core is derived from the measured pressure trace in the period between compression and the point where significant heat release occurs, after this point the specific volume is extrapolated exponentially thereafter [19, 75]. This method faithfully reproduces the specific volume of the reactive mixture during compression and during the initial stage of the ignition process, when heat release is marginal, as shown by comparison with measurement on non-reactive mixtures in [19]. Figure 5 presents the experimental pressure trace and the calculated ignition delay time. As can be seen, the calculated pressure trace faithfully reproduces the experimental trace in the period prior to ignition. For more details about this simulation procedure we refer to [19, 75].

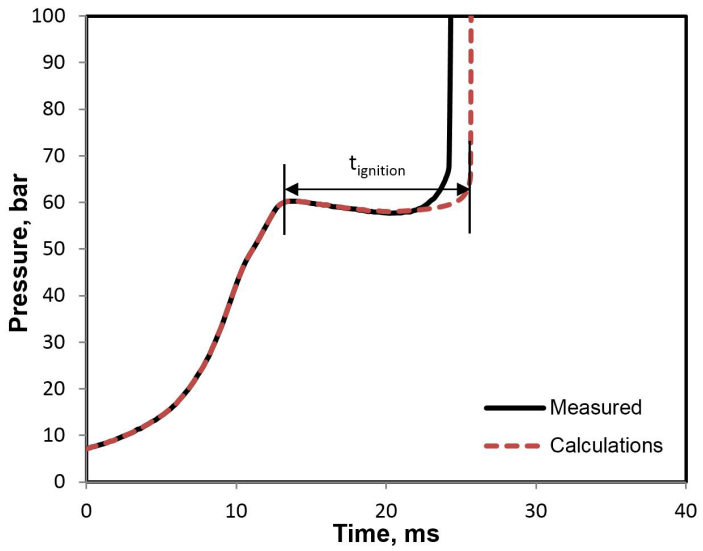

Figure 5: Pressure trace for mixture B (Table 3) at T_c=930 K: Experimental pressure (solid line), calculated pressure (dashed line).

4. Results and discussion

4.1. Oxidation in the flow reactor

The major aim of this work was to characterize ethane oxidation at high pressures and intermediate temperatures. The results from the flow-reactor measurements at temperatures of 600–900 K and pressures of 20–100 bar are presented in this section. The gas residence time at the isothermal part of the reactor was estimated to be 3–4 s, 7–10 s, and 14–22 s for pressures of 20, 50, and 100 bar, respectively. For simulations, the temperature profiles (provided as supplementary material) were implemented to improve the accuracy. The tests were carried out on stoichiometric, strongly reducing, and strongly oxidizing mixtures. Evaluating models under very fuel-rich and fuel-lean conditions can reveal the deficiency of subsets of the mechanism that are only sensitive under specific circumstances.

Figure 6 presents the results of experiments for fuel-rich mixtures (ϕ=37–47) at pressures of 20, 50, and 100 bar. At 20 bar pressure the fuel consumption starts at 775 K. Ethene and to a lesser extent CO and CH_4 are the major products. Increasing pressure to 50 and then 100 bar shifts the onset temperatures of the fuel conversion to 750 and 700 K, respectively. The gas residence time in the isothermal zone of the reactor increases by about a factor of five when the pressure is increased from 20 to 100 bar. However, the

fuel conversion in the higher end of the temperature range is inhibited by increasing pressure, reflected in the lower yield of C_2H_4. As outlined earlier, separating methanol and acetaldehyde is not possible due to overlapping GC signals, so only the the total yield of methanol plus acetaldehyde is quantified. This yield initially increases but soon decreases with increasing temperature and it is independent of pressure at higher temperatures.

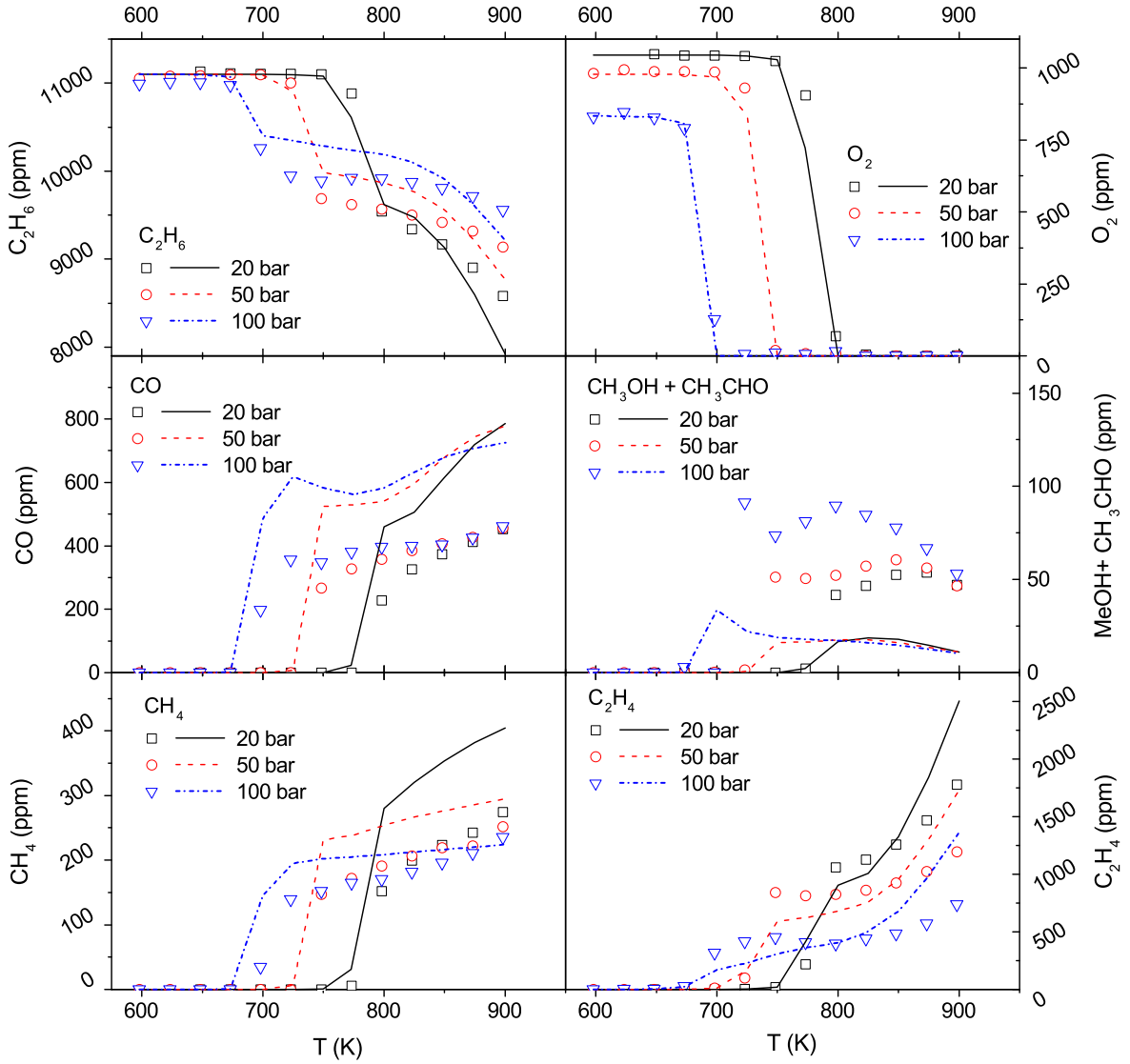

Figure 6: Results (molar fractions) of experiments under reducing conditions at 20 bar (ϕ=37.2, 11130/1044 ppm of C_2H_6/O_2), 50 bar (ϕ=39.7, 11055/978 ppm of C_2H_6/O_2), and 100 bar (ϕ=46.6, 10990/834 ppm of C_2H_6/O_2). All mixtures are diluted in nitrogen. Symbols mark experimental results and lines denote predictions of the present model using the temperature profiles in the supplementary materials. Approximating the gas residence time by τ=2525 / T [K] s (20 bar), τ=6204 / T [K] s (50 bar), and τ=12970/T [K] s (100 bar) may deteriorate the model predictions slightly.

The results under reducing conditions could indicate that ethane is oxidized in two stages. The fuel is consumed rapidly in the first stage, while as the temperature increases, the consumption of ethane becomes slow. This behavior, which is most pronounced at 100 bar, is caused by the depletion of O_2 and cannot be attributed to NTC type chemistry.

The model predictions for reducing conditions are in satisfactory agreement with measurements (Fig. 6). The model predicts the onset temperature of the fuel conversion accurately and trends are captured well. The major products, CO and CH_4, are slightly overpredicted while the sum of methanol and acetaldehyde is underpredicted. According to the model, acetaldehyde is formed to a greater extent than methanol, so the sum of them likely represents acetaldehyde formation.

For near-stoichiometric mixtures (ϕ=0.81–0.91), the onset of fuel oxidation is shifted to higher temperatures of 825, 775, and 750 K for pressures of 20, 50, and 100 bar, respectively (Fig. 7). The major products are CO, CO_2 and C_2H_4, with C_2H_4 disappearing at increased temperature. The model predictions agree very well with the measurements.

For fuel-lean mixtures ($\phi = 0.034$–0.038) (Fig. 8), the fuel oxidation starts at temperatures close to those found for stoichiometric mixtures. Here, the major products are CO and CO_2. Similar to stoichiometric conditions, C_2H_4 peaks at intermediate temperatures and disappears at higher temperatures.

From the experiments, it can be seen that when pressure and residence time are increased, the fuel oxidation starts at lower temperatures. To separate the effects of residence time from pressure, ethane conversion for different fuel-air equivalence ratios at a fixed residence time is studied using the model (see Supplemental Material). For reducing conditions, increasing pressure facilitates ignition at lower temperatures, but inhibits the conversion at 900 K. For stoichiometric and oxidizing conditions, higher pressures promote ignition and conversion. The predicted promoting effect of pressure on ignition is in line with the findings of Hunter et al. [4] who studied ethane oxidation at pressures up to 10 atm and temperatures around 925 K. The same trend was also found by Rasmussen et al. [22] for mixtures of methane and ethane.

The reaction pathways for ethane consumption at 100 bar and 700–775 K are shown in Fig. 9. The first step in ethane oxidation is H-abstraction by OH to form an ethyl

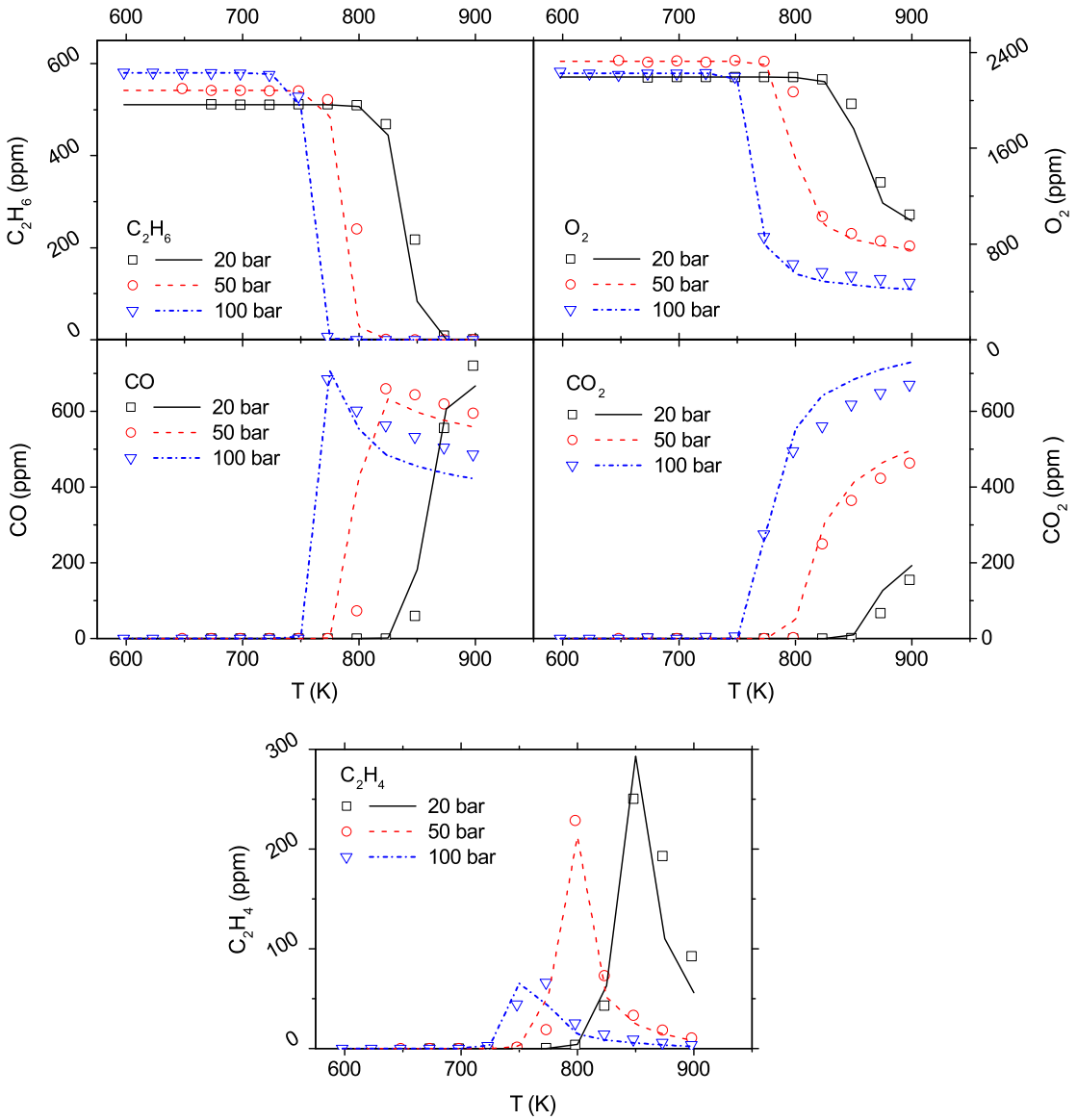

Figure 7: Results (molar fractions) of experiments under stoichiometric conditions at 20 bar (ϕ=0.82, 511/2194 ppm of C_2H_6/O_2), 50 bar (ϕ=0.81, 542/2328 ppm of C_2H_6/O_2), and 100 bar (ϕ=0.91, 580/2228 ppm of C_2H_6/O_2). All mixtures are diluted in nitrogen. Symbols mark experimental results and lines denote predictions of the present model using the temperature profiles in the supplementary materials. Approximating the gas residence time by τ=2580/T [K] s (20 bar), τ=6170/T [K] s (50 bar), and τ=12830/T [K] s (100 bar) may deteriorate the model predictions slightly.

radical. At the early stages of oxidation, also the abstraction by HO_2 is important.

$$C_2H_6 + OH \rightleftharpoons C_2H_5 + H_2O \quad \text{(R4)}$$

$$C_2H_6 + HO_2 \rightleftharpoons C_2H_5 + H_2O_2 \quad \text{(R5)}$$

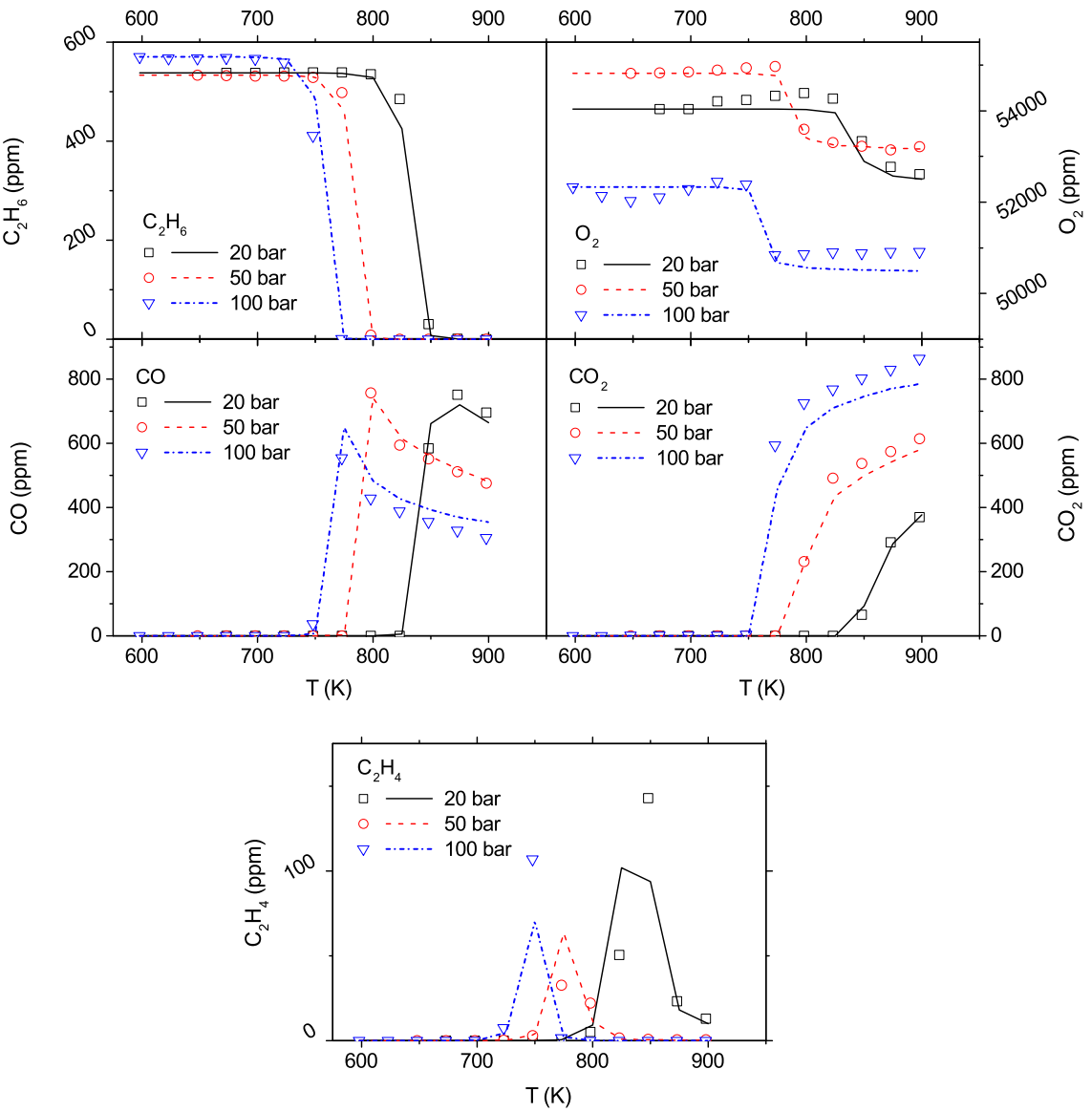

Figure 8: Results (molar fractions) of experiments under oxidizing conditions at 20 bar (ϕ=0.035, 538/54035 ppm of C_2H_6/O_2), 50 bar (ϕ=0.034, 533/54815 ppm of C_2H_6/O_2), and 100 bar (ϕ=0.038, 570/52335 ppm of C_2H_6/O_2). All mixtures are diluted in nitrogen. Symbols mark experimental results and lines denote predictions of the present model using the temperature profiles in the supplementary materials. Approximating the gas residence time by τ=2327/T [K] s (20 bar), τ=5950/T [K] s (50 bar), and τ=11890/T [K] s (100 bar) may deteriorate the model predictions slightly.

The ethyl radical adds to molecular oxygen to form CH_3CH_2OO, which dissociates to

ethene and a hydroperoxyl radical,

$$C_2H_5 + O_2(+M) \rightleftharpoons CH_3CH_2OO(+M) \quad \text{(R12a)}$$

$$CH_3CH_2OO(+M) \rightleftharpoons C_2H_4 + HO_2(+M) \quad \text{(R13b)}$$

Under reducing conditions, recombination of C_2H_4 and H is favoured compared to C_2H_4 oxidation, so ethene becomes a major final product of the process, as seen in Fig 6. A minor but important fraction of CH_3CH_2OO reacts with HO_2 to form CH_3CH_2OOH;

$$CH_3CH_2OO + HO_2(+M) \rightleftharpoons CH_3CH_2OOH + O_2(+M) \quad \text{(R14)}$$

which then dissociates to ethoxy (CH_3CH_2O). The ethoxy radical decomposes to a methyl radical and formaldehyde.

$$CH_3CH_2OOH(+M) \rightleftharpoons CH_3CH_2O + OH(+M) \quad \text{(R16)}$$

$$CH_3CH_2O(+M) \rightleftharpoons CH_2O + CH_3(+M) \quad \text{(R17)}$$

Under stoichiometric and oxidizing conditions, the fuel consumption proceeds partly through association of C_2H_4 with OH to CH_2CH_2OH, which itself adds to molecular oxygen,

$$C_2H_4 + OH(+M) \rightleftharpoons CH_2CH_2OH(+M) \quad \text{(R18a)}$$

$$CH_2CH_2OH + O_2(+M) \rightleftharpoons HOCH_2CH_2OO(+M) \quad \text{(R20)}$$

The resulting $HOCH_2CH_2OO$ radical then dissociates to form formaldehyde.

As discussed above, the reaction pathways found under these conditions are different from the general pathways suggested for larger alkanes [40], as the isomerization of CH_3CH_2OO to CH_2CH_2OOH (R13a) is not competitive with thermal dissociation to $C_2H_4 + HO_2$ (R13b).

The sensitivity of the modelling predictions to the rate constants of the reactions is

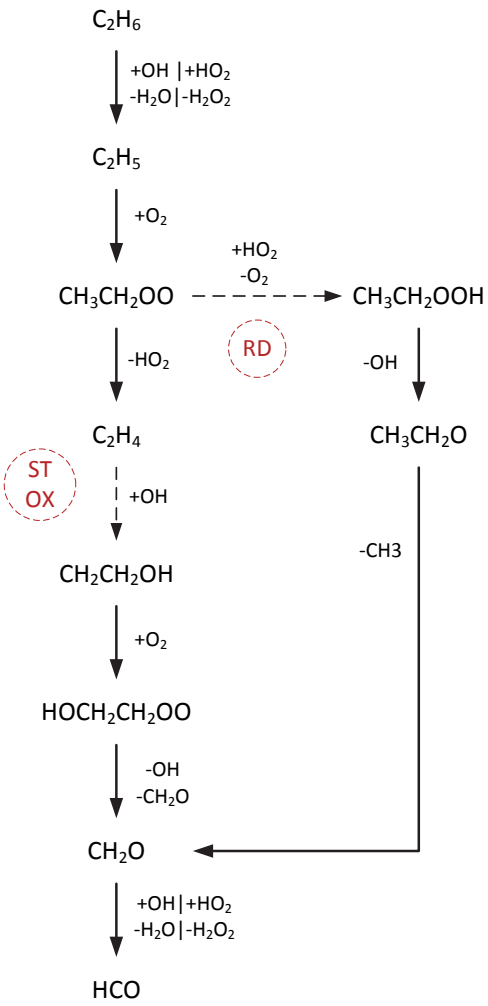

Figure 9: The major consumption path of ethane in the flow reactor at 100 bar pressure upon onset of reaction (700–775 K) under reducing (RD), stoichiometric (ST), and oxidizing (OX) conditions.

analysed via a brute-force method. Here, the sensitivity coefficient (S_i) is defined as

$$S_i = \frac{\left(\Delta X_{\mathrm{C_2H_6}}/X_{\mathrm{C_2H_6}}\right)}{\left(\Delta k_i/k_i\right)} \tag{2}$$

where k_i is the rate constant of the ith reaction. Figure 10 shows the results of the analysis at 100 bar. The dissociation of H_2O_2 to OH,

$$\mathrm{H_2O_2(+M) \rightleftharpoons OH + OH(+M)} \tag{R21}$$

is the most sensitive reaction. The H-abstraction by HO_2 (R5) is another controlling step upon the ignition at 100 bar.

Hydrogen abstraction reactions involving CH_3CH_2OO and CH_3OO are important, in

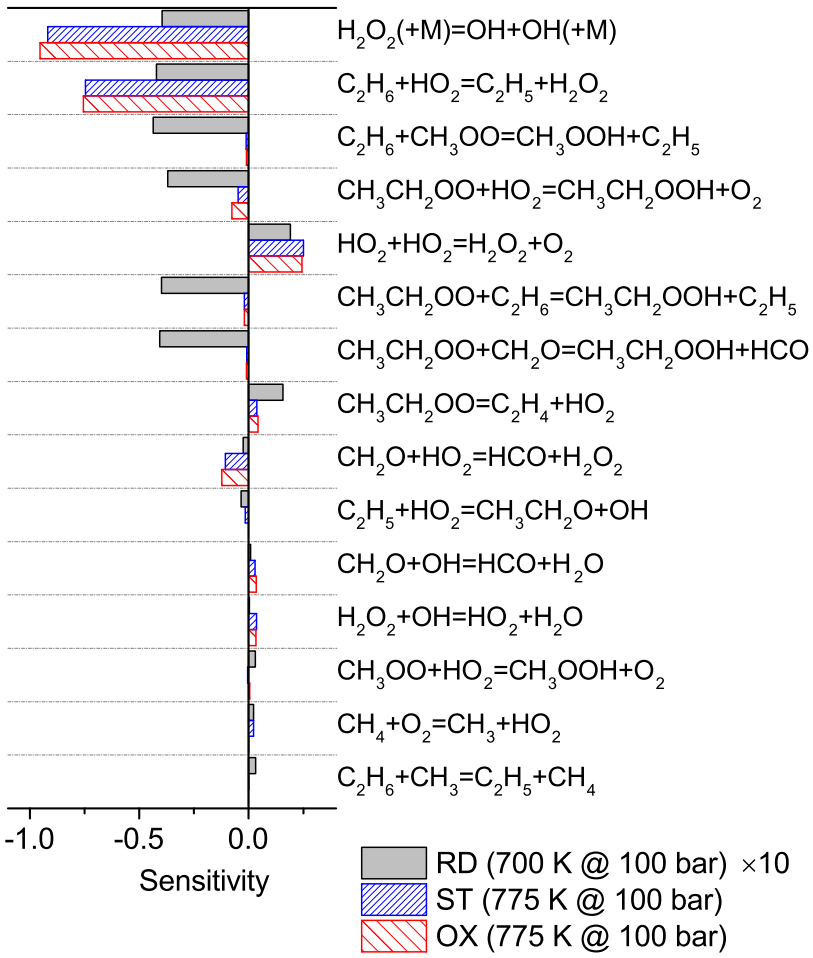

Figure 10: Sensitivity coefficients of C_2H_6 molar fraction. The coefficients are calculated at a residence time corresponding to 20% conversion of either C_2H_6 or O_2 (whichever happens earlier). Negative coefficients indicate promoting effect on fuel conversion.

particular under reducing conditions.

$$CH_3CH_2OO + HO_2 \rightleftharpoons CH_3CH_2OOH + O_2 \quad \text{(R14)}$$

$$CH_3CH_2OO + C_2H_6 \rightleftharpoons CH_3CH_2OOH + C_2H_5 \quad \text{(R22)}$$

$$CH_3OO + C_2H_6 \rightleftharpoons CH_3OOH + C_2H_5 \quad \text{(R23)}$$

$$CH_3CH_2OO + CH_2O \rightleftharpoons CH_3CH_2OOH + HCO \quad \text{(R24)}$$

This is in line with our expectation of a dominant role of these compounds at high pressures and intermediate temperatures.

4.2. Ignition in the RCM

Autoignition experiments in the RCM have been conducted at temperatures ranging from 900–1025 K and pressures of 10–80 bar, extending the range of conditions covered by the flow reactor data. The experimental results are presented in Figs. 11–15.

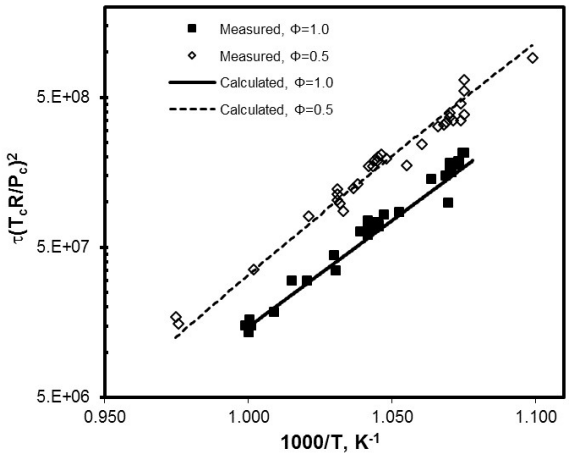

Figure 11: Measured ignition delay times (dots) and calculated ignition delay times (lines) scaled to second-order with the reciprocal density and plotted as function of the reciprocal temperature (T_c) for stoichiometric (mixture A) and the fuel lean, Φ=0.5 (mixture B) mixtures.

To present all the results in one figure, the auto-ignition delay times measured at different temperature (T_c) and pressure (P_c) are scaled to second order with the reciprocal density and plotted as a function of the reciprocal temperature (T_c) for the fuel lean (Φ=0.5) and stoichiometric mixtures in Fig. 11 similar to the scaling done in [75]. It can be seen from Fig. 11 that the measured ignition delay times at Φ=0.5 are systematically longer, about a factor of two, than those observed at Φ=1.0. Also interesting to note is

that the slope of the lines at Φ=0.5 and Φ=1.0 are almost identical, which suggests a similar overall activation energy for both equivalence ratios, as also observed in [11] where the measurements were performed in the high temperature regime (T=1235–1660 K). However, we refrain from further analyses of the apparent activation energy due to varying degrees of heat loss in the pre-ignition period for different times. In contrast to the results shown here, the authors in [11, 18] observed that an increase in equivalence ratio resulted in an increase in the autoignition delay time in the high temperature regime.

Figures 12 and 13 show the autoignition delay times, measured along the isotherm at $T_c \simeq$932 K (Fig. 12) and $T_c \simeq$958 K (Fig. 13) at fuel lean and stoichiometric conditions. The scatter observed along the two isotherms is mainly caused by day-to-day variations in the compressed temperature (±4 K) in the measurements. From Figs. 12 and 13 it can be seen that increasing the pressure from 20 to 40 bar results in a reduction of the autoignition delay time by about a factor of 3.5 for all measurements; this promoting effect of pressure is in qualitative agreement with the flow reactor measurements at stoichiometric conditions. In addition, the substantially shorter times measured for stoichiometric mixtures than for lean mixtures are clearly seen in the figures. From Fig. 14 it can be seen that increasing the temperature over the measured domain of ∼70 K, at a constant pressure of 30 bar, results in a reduction of the autoignition delay time by roughly an order of magnitude.

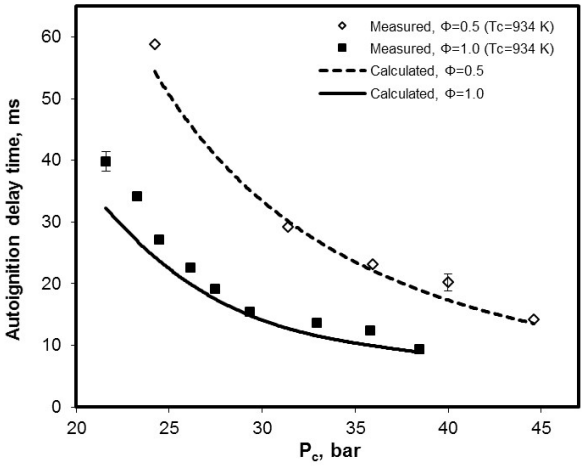

Figure 12: Measured (symbols) and calculated (lines) autoignition delay times plotted as function of pressure (P_c) at fixed peak compression temperature T_c ∼934 K at stoichiometric and fuel lean conditions,Φ=0.5.

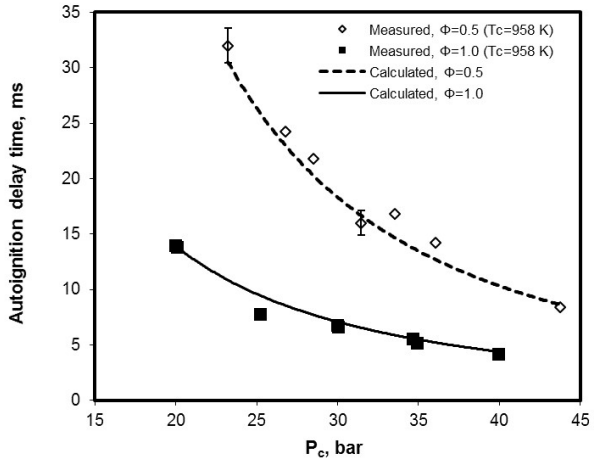

Figure 13: Measured (symbols) and calculated (lines) autoignition delay times plotted as function of pressure (P_c) at fixed peak compression temperature T_c=958 K at stoichiometric and fuel lean conditions, Φ=0.5.

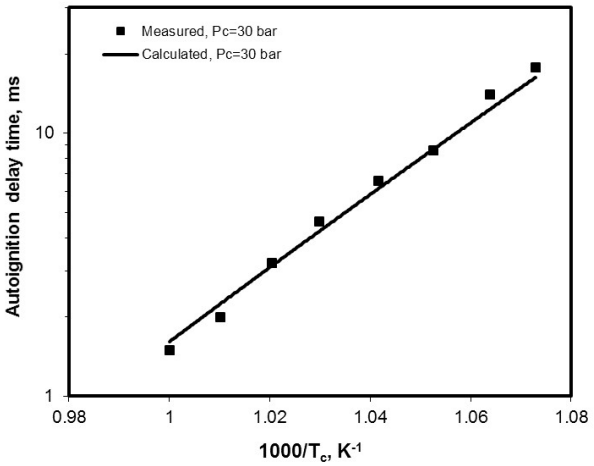

Figure 14: Measured (symbols) and calculated (lines) autoignition delay times plotted as function of temperature (T_c) at fixed peak compression pressure, P_c ~30 bar, at stoichiometric conditions.

Figure 15 shows the isotherms measured at 930 and 970 K from 40–80 bar at fuel lean conditions, extending the experimental maximum pressure by a factor of two from Figs. 12 and 13. The results show the continued reduction in the autoignition delay time with increasing pressure.

The computational results shown in Figs. 11-15 are presented as polynomial trend lines through the computed points to avoid clutter in the figures. As can be seen in Fig. 11, the calculated ignition delay times, scaled to second-order with the reciprocal density, reproduce the trends in ignition delay time faithfully at stoichiometric and fuel-lean conditions for the entire range of temperatures studied. From Figs. 12–15 it can

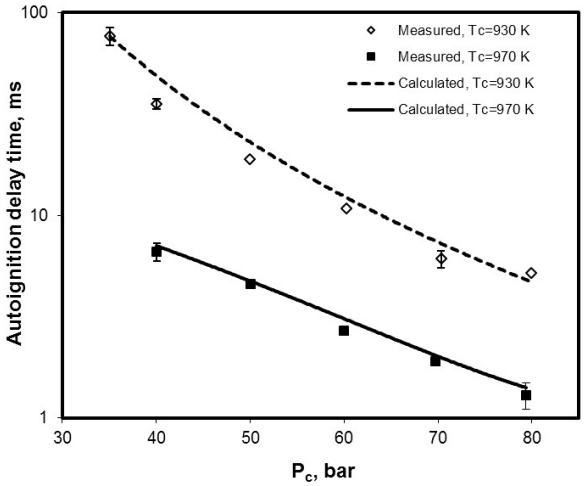

Figure 15: Measured (symbols) and calculated (lines) autoignition delay times plotted as function of pressure (P_c) at fixed peak compression temperature Tc ~930 K and T_c ~970 K for fuel lean mixtures Φ=0.5 (Mixture B, Table 3).

be seen that the agreement between measurements and calculations is generally better than 15% for the entire range of pressures and temperatures. However, for stoichiometric conditions at pressure below 30 bar the modelling predictions are less accurate (Fig. 14), with an underprediction of the ignition delay of up to 30%.

The sensitivity analyses presented in Fig. 16 are performed at the pressures P_c=20 bar and P_c=80 bar for the isotherm T_c=930 K, corresponding to the conditions in Fig. 15. Although the magnitude of the sensitivity coefficients differs for the individual reactions, the autoignition delay time is sensitive to the same subset of reactions for both pressure conditions. Furthermore, sensitivity and rate of production analyses show that the H-abstraction from ethane by hydroperoxyl (R4) is important for promoting the autoignition, similar to what was observed at the flow reactor conditions described above. Additionally, from Fig. 16 it can be seen that the peroxide chemistry is important. The reactions

$$H_2O_2(+M) \rightleftharpoons OH + OH(+M) \quad \text{(R21)}$$

$$CH_3CH_2OOH + O_2 \rightleftharpoons CH_3CH_2OO + HO_2 \quad \text{(R25)}$$

$$CH_3CH_2OOH + C_2H_5 \rightleftharpoons CH_3CH_2OO + C_2H_6 \quad \text{(R26)}$$

act to promote ignition, while

$$HO_2 + HO_2 \rightleftharpoons H_2O_2 + O_2 \qquad \text{(R27)}$$

inhibits the ignition process.

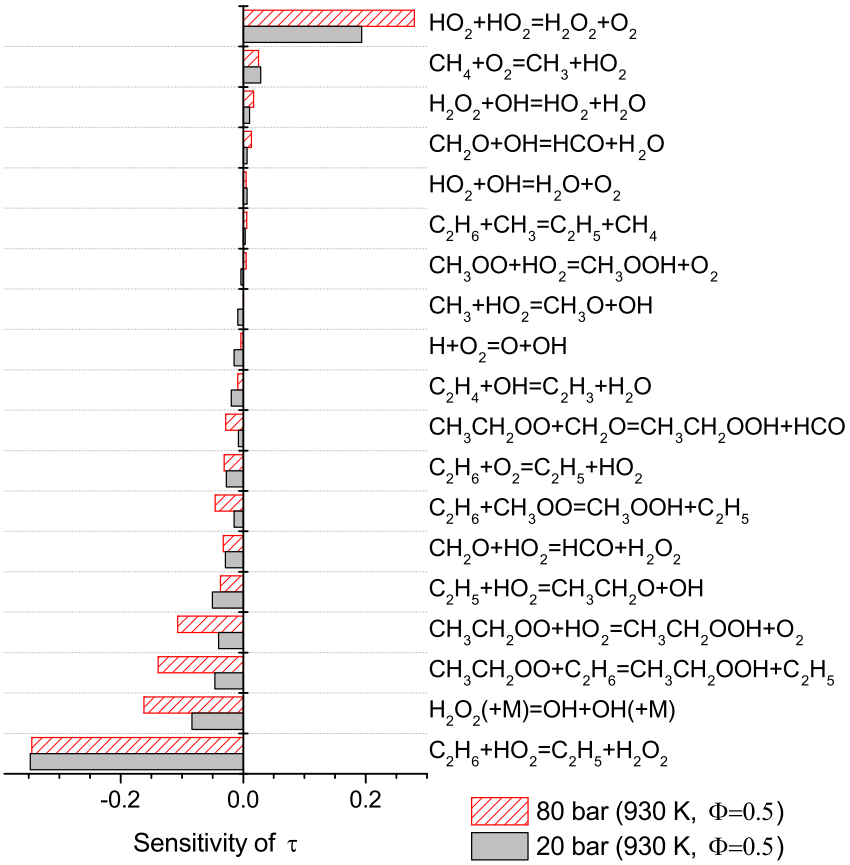

Figure 16: Sensitivity coefficients with respect to the auto ignition delay time calculated at T_c=930 K and P_c=20 bar (blue bars) and P_c=80 bar (red bars) at fuel lean conditions, Φ=0.5. Negative coefficients indicate faster ignition.

4.3. Comparison with literature data

Above, the chemical kinetic model was evaluated against data from the flow reactor experiments at pressures of 20–100 bar and temperatures of 600–900 K and from the RCM at pressures of 20–80 bar and temperatures of 800–1025 K. To assess further the possibility of NTC behavior for ethane, data on high-pressure explosion limits from batch reactor experiments are interpreted in terms of the detailed model. In addition, the model evaluation is extended to higher temperatures by comparison to data from shock tubes and flame measurements in the following sections.

4.3.1. High-pressure explosion limits

Experimental data for explosion limits of ethane have been reported in several studies [35–39]. As discussed above, results are not conclusive but the experiments differ significantly with respect to reactor material and size, stoichiometry, pressure, and temperature. Here we focus on the data obtained by Townend and coworkers [37, 38] at elevated pressure (2-25 atm) and temperatures in the 600-800 K range.

Figure 17 compares the measured explosion limits for a mixture of 10% ethane in air with predictions by the present model. From 800 K down to about 705 K, Townend and Chamberlain [37] report a smooth increase in explosion pressure. However, at 710 K there is a sharp inflection point. Between 710 and 620 K, the explosion pressure is almost constant; below 620 K it then increases rapidly.

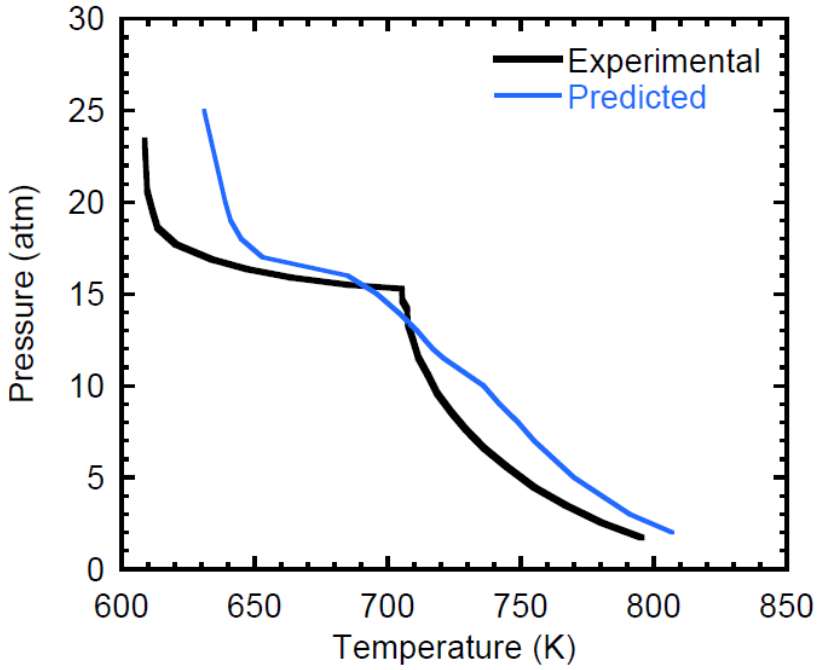

Figure 17: Measured and predicted explosion limits for C_2H_6/air mixtures. The thick black solid curve marks experimental results from Townend and Chamberlain [37] for a mixture with 10% ethane, while the blue curve presents the predicted results.

The experiments were conducted in a reactor with a mild steel liner and despite the enhanced pressure, some surface interaction would be anticipated. Surface effects would presumably be most pronounced at temperatures below the inflection point where ignition times were reported to increase dramatically, from being of the order of a minute at the higher temperatures to two hours at the lowest investigated temperatures. For clarity,

we did not include a wall termination reaction in the modeling; instead explosion had to occur within a set induction time under isothermal conditions to be acknowledged. The limiting induction time was somewhat arbitrarily set to 10 s; the use of a different value would affect the predicted explosion limits but not the overall trends.

Considering the experimental uncertainties and the simplifications in the modeling, the calculations are in satisfactory agreement with observations. Explosion pressures are predicted satisfactorily above 650 K; below this temperature reported induction times were excessively long. Also the inflection point is captured by the model, even though it is not as sharp as the measured one.

The reaction pathways are similar to those outlined in Fig. 9 for reducing conditions. Ethane is converted through ethyl peroxide, $C_2H_6 \xrightarrow{+OH} C_2H_5 \xrightarrow{+O_2} CH_3CH_2OO \xrightarrow{+HO_2,CH_2O} CH_3CH_2OOH$, followed by the chain branching sequence $CH_3CH_2OOH(+M) \rightarrow CH_3CH_2O+OH(+M)$ (R16), $CH_3CH_2O(+M) \rightarrow CH_2O+CH_3(+M)$ (R17). The development of the radical pool is quite sensitive to the fate of CH_3CH_2OO. Hydrogen abstraction reactions forming CH_3CH_2OOH (R14, R22, R24) promote chain-branching, while thermal dissociation, $CH_3CH_2OO(+M) \rightarrow C_2H_4+HO_2(+M)$ (R13b) is in effect chain-terminating. The dissociation of CH_3CH_2OO (R13b) is in the fall-off region under these conditions (see Arrhenius plot in the Supplemental Material). As the pressure increases, k_{13b} approaches the high-pressure limit and the reaction becomes less competitive compared to the bimolecular steps (R14, R22, R24) that lead to branching and explosion. Conceivably the sharper inflection observed experimentally is augmented by the pressure-dependent competition for HO_2 between reaction and diffusion to the wall (termination). However, the inflection point and the plateau in explosion pressure at 650-700 K are not caused by NTC-type chemistry, i.e., $CH_3CH_2OO \longrightarrow CH_2CH_2OOH \xrightarrow{+O_2} OOCH_2CH_2OOH \rightarrow$ *branching* since isomerization of CH_3CH_2OO (R13a) is too slow to compete.

4.3.2. Ignition delays at higher temperatures

The ignition delay time of ethane has been measured at pressures greater than 10 atm in several shock tube studies [16, 18, 83, 84]. Figure 18 shows the measured ignition delay times and the predictions by the present model. The modelling predictions generally compare reasonably well with the measured values.

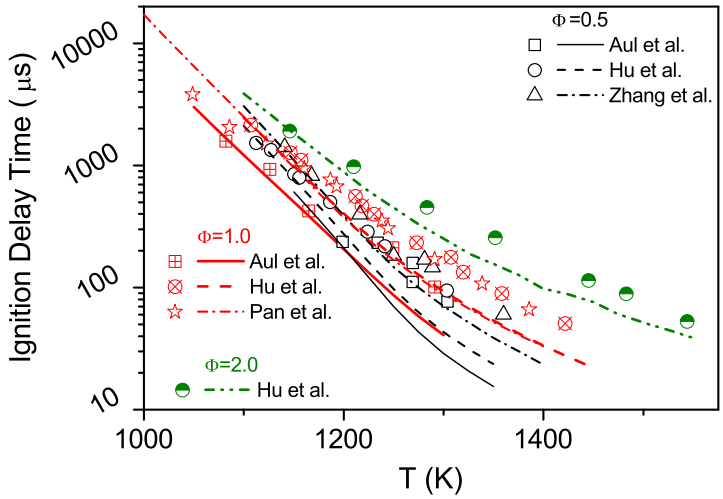

Figure 18: Ignition delay time of $C_2H_6/O_2/Ar$ mixtures calculated by the present model. Symbols mark experimental results from Aul et al. [16] (85% Ar, 16 atm), Zhang et al. [18] (95% Ar, 21 atm), Pan et al. [83] (95% Ar, 16 atm), and Hu et al. [84] (1% C_2H_6 in Ar, 20 atm).

4.3.3. Species profiles from shock tubes

Tranter and coworkers have measured the concentration of stable components behind the shock in a shock tube at high pressures of 40 [7], as well as 340 and 613 bar [6]. The post-shock composition was measured by a GC. By recording pressure and calculating temperature accordingly, they were able to simulate the post-shock conditions.

To simulate the data, here a fixed pressure (40, 340, and 613 bar) and a residence time of 1.7 ms were implemented in the model. As shown in Fig. 19 for 40 bar, the fuel conversion starts around 1150 K and is accompanied by a gradual increase in the concentrations of CO and C_2H_4. Above 1250 K, the C_2H_4 concentration decreases and it almost disappears around 1400 K. At 340 and 613 bar, the fuel conversion is detected above 1075 K. The model generally agrees well with the measurements, even though at 340 bar the temperature for onset of oxidation is overpredicted by around 50 K.

4.3.4. Flame speeds

Laminar flame speeds of combustible mixtures are widely used to evaluate kinetic models. For ethane/air mixtures, the flame speed has been measured at pressures up to 10 atm [26, 85–90]. Figure 20 compares modelling predictions with measurements at 1, 5, and 10 atm. Following Law et al. [91], we plot the burning velocities against normalized fuel-air equivalence ratio for a better representation. The model overpredicts the flame

speed by up to about 5 cm s^{-1} for fuel-lean and stoichiometric mixtures, but its accuracy improves for fuel-rich mixtures.

The reason for the overprediction of the ethane flame speed is not clear. The present model predicts the flame speeds of hydrogen, methane, and acetylene very well [27, 29, 31]. The calculated flame speeds of ethene and acetylene are shown in figure 21 for atmospheric pressure and the results are within the uncertainty range of the experimental measurements. Sensitivity analyses are conducted using built-in functions of CHEMKIN [74] for mass flow rate sensitivity, which represents well the sensitivity of flame speed to reaction rate constants. Results of the analyses for ethane, ethene, and acetylene flames are shown in Fig. 22.

Only two reactions show up as controlling the predicted ethane flame speed but not important in calculating flame speeds of ethene and acetylene:

$$C_2H_5(+M) \rightleftharpoons C_2H_4 + H(+M) \qquad \text{(R8(b))}$$

$$C_2H_5 + H \rightleftharpoons CH_3 + CH_3 \qquad \text{(R9(b))}$$

In ethane flames, reaction R8(b) produces H atoms while reaction R9(b) consumes H. Earlier, Park et al. [96] examined three chemical kinetic models and found that all of them overpredicted the flame speed of ethane. Park et al. [96] concluded that inaccuracies in the rate constants for reactions R8(b) and R9(b) may be a reason for the disagreement between the models and measurements for ethane flame speed. However, for both reactions rate coefficients seem to be fairly well established. For k_8, we relied on a theoretical study by Miller and Klippenstein [61], which is in good agreement with measured data. The rate constant for reaction R9 was taken from the evaluation of Baulch et al. [57].

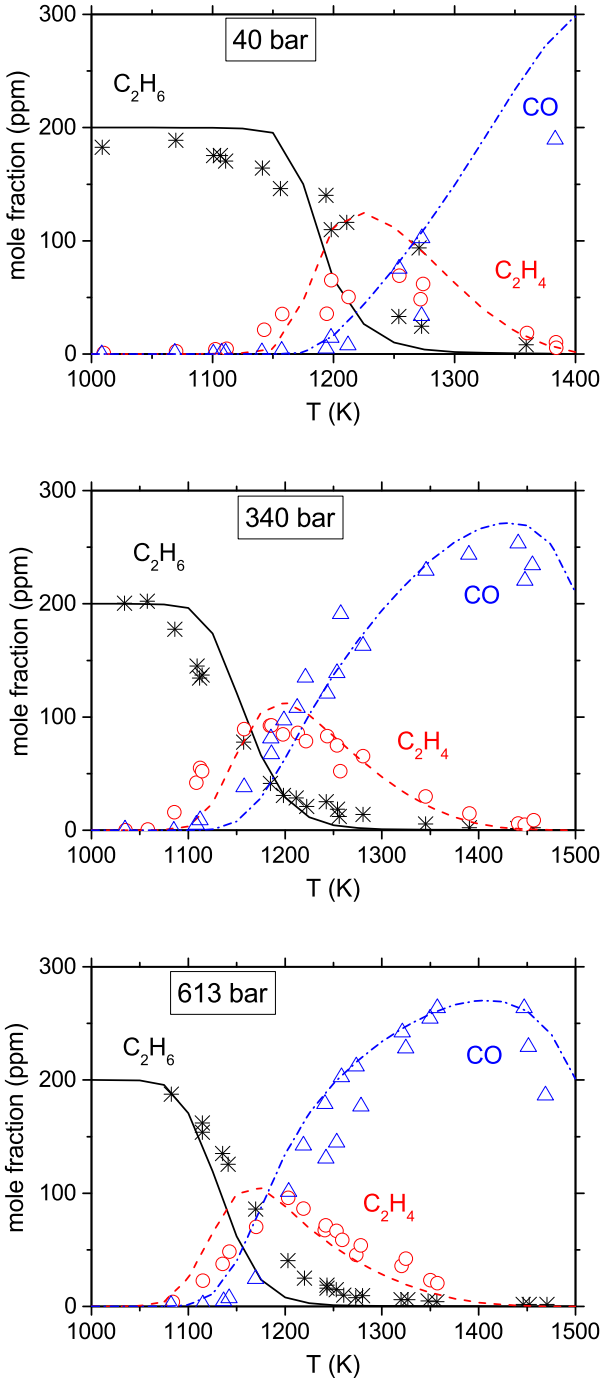

Figure 19: Post–shock concentration profiles at different temperatures. Symbols mark experimental results measured in a shock tube with initial mole fractions of 200 ppm of C_2H_6 (Φ=1, in AR) at pressures of Top: 40 bar, from ref [7]; Middle: 340 bar, from ref [6]; Bottom: 613 bar, from ref [6]. Lines denote the prediction of the present model implementing a fixed residence time of 1.7 ms.

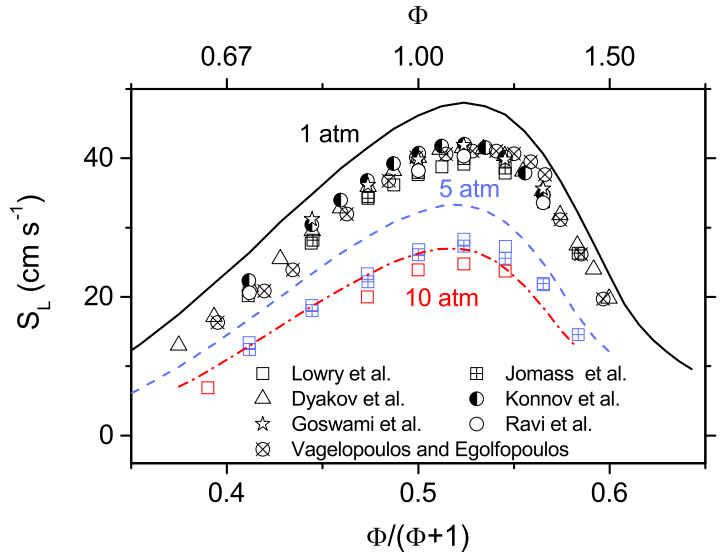

Figure 20: The unstretched laminar burning velocity of ethane/air mixtures versus normalized equivalence ratio for an initial temperature of 300 K and at different pressures. Lines denote the present model predictions and symbols mark experimental results from Ravi et al. [26], Vagelopoulos and Egolfopoulos [85], Konnov et al. [86], Jomaas et al. [87], Dyakov et al. [88], Lowry et al. [89], Goswami [90].

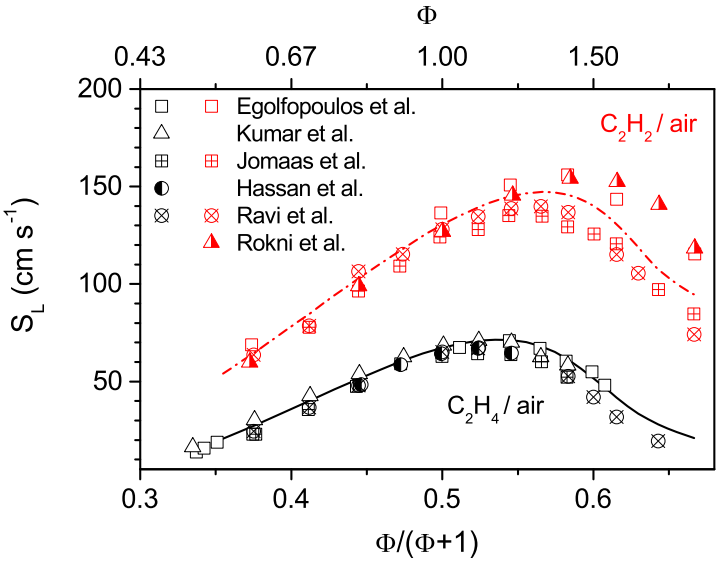

Figure 21: The unstretched laminar burning velocity of ethene/air and acetylene/air mixtures versus normalized equivalence ratio for an initial temperature of 300 K and at atmospheric pressure. Lines denote the present model predictions and symbols mark experimental results from Ravi et al. [26], Jomaas et al. [87], Egolfopoulos et al. [92], Hassan et al. [93], Kumar et al. [94], and Rokni et al. [95].

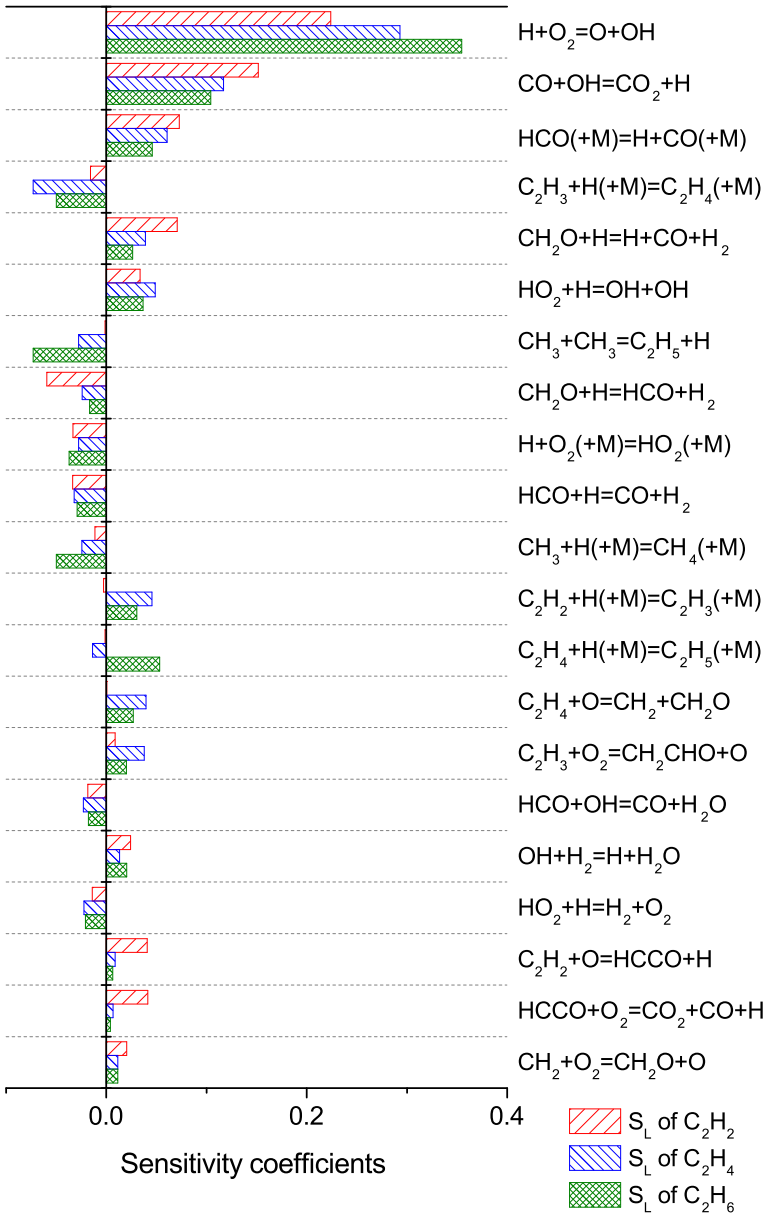

Figure 22: The sensitivity of the mass flow rate of the stoichiometric mixtures of ethane, ethene, and acetylene in air at atmospheric pressure and initial temperature of 300 K.

5. Conclusion

Ethane oxidation was investigated in a laminar flow reactor at intermediate temperatures of 600–900 K and high pressures of 20–100 bar. In the experiments, the concentrations of stable species were measured at the reactor outlet while temperature was varied. The results revealed onset temperatures of reaction between 700 K and 825 K, depending on pressure and stoichiometry. The onset temperature decreased with increasing pressure, with no indication of NTC behavior, while stoichiometry had only a minor effect. The RCM experiments, conducted at temperatures of 900–1025 K and pressures of 10–80 bar, showed that the ignition delay time decreased substantially with increasing pressure and temperature. Ignition delays at ϕ=0.5 were longer than at ϕ=1.0.

A detailed chemical kinetic model was developed with particular attention to the peroxide chemistry. Rate constants for reactions on the $C_2H_5O_2$ potential energy surface were adopted from the recent theoretical work of Klippenstein and the internal H-abstraction in CH_3CH_2OO to form CH_2CH_2OOH was studied at a high level of theory. Our work did not support occurrence of NTC behavior in ethane oxidation. Even at the high-pressure conditions of the present work where the $C_2H_5 + O_2$ reaction yields ethylperoxyl rather than $C_2H_4 + HO_2$, the chain branching sequence $CH_3CH_2OO \longrightarrow CH_2CH_2OOH \xrightarrow{+O_2} OOCH_2CH_2OOH \rightarrow$ *branching* is not competitive, because the internal H-atom transfer in CH_3CH_2OO to CH_2CH_2OOH is too slow compared to thermal dissociation to C_2H_4 and HO_2.

Modeling predictions for species concentrations from the flow reactor experiments and ignition delay times from the RCM were satisfactory. In addition, the model could reproduce ignition delay times and post-shock concentrations from shock-tube experiments in literature, but it overpredicted flame speed at pressures of 1–5 bar.

The data provided extend the ethane oxidation benchmark at high pressures and intermediate temperatures. Models validated against such data can be used more safely in the optimization of engines and gas turbines.

Acknowledgement

Funding from the *European Graduate School* as well as *MAN Diesel & Turbo* is gratefully acknowledged. This project has received funding from the *European Union's Horizon*

2020 research and innovation programme under grant agreement No 634135. Part of this material is based on work at Argonne supported by the U.S. Department of Energy, Office of Basic Energy Sciences, Division of Chemical Sciences, Geosciences, and Biosciences, under Contract No. DE-AC02-06CH11357 as part of the Argonne-Sandia Consortium on High-Pressure Combustion Chemistry, (ANL FWP # 59044). Finally, the article is partly based upon work from COST Action SMARTCATs (CM1404), supported by COST (European Cooperation in Science and Technology, www.cost.eu)

6. References

[1] J. Huang, W. Bushe, Experimental and kinetic study of autoignition in methane/ethane/air and methane/propane/air mixtures under engine-relevant conditions, Combust. Flame 144 (2006) 74–88.

[2] S. Tanaka, F. Ayala, J. C. Keck, J. B. Heywood, Two-stage ignition in HCCI combustion and HCCI control by fuels and additives, Combust. Flame 132 (2003) 219–239.

[3] J. Y. Ren, F. N. Egolfopoulos, T. T. Tsotsis, NO_x emission control of lean methane-air combustion with addition of methane reforming products, Combust. Sci. Technol. 174 (2002) 181–205.

[4] T. B. Hunter, T. A. Litzinger, H. Wang, M. Frenklach, Ethane oxidation at elevated pressures in the intermediate temperature regime: Experiments and modeling, Combust. Flame 104 (1996) 505–523.

[5] P. Dagaut, M. Cathonnet, J.-c. Boettner, Kinetics of ethane oxidation, Int. J. Chem. Kinet. 23 (1991) 437–455.

[6] R. S. Tranter, R. Sivaramakrishnan, K. Brezinsky, M. D. Allendorf, High pressure, high temperature shock tube studies of ethane pyrolysis and oxidation, Phys. Chem. Chem. Phys. 4 (2002) 2001–2010.

[7] R. S. Tranter, H. R. Amoorthy, A. Raman, K. Brezinsky, M. D. Allendorf, High-pressure single-pulse shock tube investigation of rich and stoichiometric ethane oxidation, Proc. Combust. Inst. 29 (2002) 1267–1275.

[8] R. S. Tranter, A. Raman, R. Sivaramakrishnan, K. Brezinsky, Ethane oxidation and pyrolysis from 5 bar to 1000 bar: Experiments and simulation, Int. J. Chem. Kinet. 37 (2005) 306–331.

[9] C. T. Bowman, An experimental and analytical investigation of the high-temperature oxidation mechanisms of hydrocarbon fuels, Combust. Sci. Technol. 2 (1970) 161–172.

[10] A. Burcat, K. Scheller, A. Lifshitz, Shock-tube investigation of comparative ignition delay times for C_1–C_5 alkanes, Combust. Flame 16 (1971) 29–33.

[11] A. Burcat, R. W. Crossley, K. Scheller, G. B. Skinner, Shock tube investigation of ignition in ethane-oxygen-argon mixtures, Combust. Flame 18 (1972) 115–123.

[12] D. F. Cooke, A. Williams, Shock-tube studies of methane and ethane oxidation, Combust. Flame 24 (1975) 245–256.

[13] Y. Hidaka, Y. Tanaka, H. Kawano, M. Suga, Mass spectrometric study of C_2-hydrocarbons oxidation in shock waves, J. Mass Spectrom. Soc. Jpn. 29 (1981) 191–198.

[14] N. Lamoureux, C. E. Paillard, V. Vaslier, Low hydrocarbon mixtures ignition delay times investigation behind reflected shock waves, Shock waves 11 (2002) 309–322.

[15] J. de Vries, J. M. Hall, S. L. Simmons, M. J. A. Rickard, D. M. Kalitan, E. L. Petersen, Ethane ignition and oxidation behind reflected shock waves, Combust. Flame 150 (2007) 137–150.

[16] C. J. Aul, W. K. Metcalfe, S. M. Burke, H. J. Curran, E. L. Petersen, Ignition and kinetic modeling of methane and ethane fuel blends with oxygen: A design of experiments approach, Combust. Flame 160 (2013) 1153–1167.

[17] D. J. Beerer, V. G. McDonell, An experimental and kinetic study of alkane autoignition at high pressures and intermediate temperatures, Proc. Combust. Inst. 33 (2011) 301–307.

[18] J. Zhang, E. Hu, L. Pan, Z. Zhang, Z. Huang, Shock-tube measurements of ignition delay times for the ethane/dimethyl ether blends, Energy Fuels 27 (2013) 6247–6254.

[19] S. Gersen, A. Mokhov, J. Darmeveil, H. Levinsky, P. Glarborg, Ignition-promoting effect of NO_2 on methane, ethane and methane/ethane mixtures in a rapid compression machine, Proc. Combust. Inst. 33 (2011) 433–440.

[20] D. Nötzold, J. Algermissen, Chemical kinetics of the ethane-oxygen reaction part I: High temperature oxidation at ignition temperatures between 1400 K and 1800 K, Combust. Flame 40 (1981) 293–313.

[21] C. V. Naik, A. M. Dean, Modeling high pressure ethane oxidation and pyrolysis, Proc. Combust. Inst. 32 (2009) 437–443.

[22] C. L. Rasmussen, J. G. Jakobsen, P. Glarborg, Experimental measurements and kinetic modeling of CH_4/O_2 and $CH_4/C_2H_6/O_2$ conversion at high pressure, Int. J. Chem. Kinet. 40 (2008) 778–807.

[23] G. P. Smith, D. M. Golden, M. Frenklach, N. W. Moriarty, B. Eiteneer, M. Goldenberg, C. T. Bowman, R. K. Hanson, S. Song, J. William C. Gardiner, V. V. Lissianski, Z. Qin, GRI-Mech Version 3.0, 1999. URL: `http://combustion.berkeley.edu/gri_mech/`.

[24] E. Ranzi, A. Frassoldati, R. Grana, A. Cuoci, T. Faravelli, A. P. Kelley, C. K. Law, Hierarchical and comparative kinetic modeling of laminar flame speeds of hydrocarbon and oxygenated fuels, Prog. Energy Combust. Sci. 38 (2012) 468–501.

[25] W. K. Metcalfe, S. M. Burke, S. S. Ahmed, H. J. Curran, A hierarchical and comparative kinetic modeling study of C_1–C_2 hydrocarbon and oxygenated fuels, Int. J. Chem. Kinet. 45 (2013) 638–675.

[26] S. Ravi, T. G. Sikes, A. Morones, C. L. Keesee, E. L. Petersen, Comparative study on the laminar flame speed enhancement of methane with ethane and ethylene addition, Proc. Combust. Inst. 35 (2015) 679–686.

[27] H. Hashemi, J. M. Christensen, S. Gersen, H. Levinsky, S. J. Klippenstein, P. Glarborg, High-pressure oxidation of methane, Combust. Flame 172 (2016) 349–364.

[28] S. J. Klippenstein, From theoretical reaction dynamics to chemical modeling of combustion, Proc. Combust. Inst. (2016).

[29] H. Hashemi, J. M. Christensen, S. Gersen, P. Glarborg, Hydrogen oxidation at high pressure and intermediate temperatures: Experiments and kinetic modeling, Proc. Combust. Inst. 35 (2015) 553–560.

[30] C. L. Rasmussen, J. Hansen, P. Marshall, P. Glarborg, Experimental measurements and kinetic modeling of $CO/H_2/O_2/NO$, conversion at high pressure, Int. J. Chem. Kinet. 40 (2008) 454–480.

[31] J. Lopez, C. Rasmussen, H. Hashemi, M. Alzueta, Y. Gao, P. Marshall, C. Goldsmith, P. Glarborg, Experimental and kinetic modeling study of C_2H_2 oxidation at high pressure, Int. J. Chem. Kinet. 48 (2016) 724–738.

[32] J. G. Lopez, C. L. Rasmussen, M. U. Alzueta, Y. Gao, P. Marshall, P. Glarborg, Experimental and kinetic modeling study of C_2H_4 oxidation at high pressure, Proc. Combust. Inst. 32 (2009) 367–375.

[33] V. Aranda, J. M. Christensen, M. U. Alzueta, P. Glarborg, S. Gersen, Y. Gao, P. Marshall, Experimental and kinetic modeling study of methanol ignition and oxidation at high pressure, Int. J. Chem. Kinet. 45 (2013) 283–294.

[34] H. H. Carstensen, A. M. Dean, Rate constants for the abstraction reactions RO_2 + C_2H_6; R = H, CH_3, and C_2H_5, Proc. Combust. Inst. 30 (2005) 995–1003.

[35] J. H. Knox, R. G. W. Norrish, Cool flame phenomena in the oxidation of ethane, Trans. Faraday Soc. 50 (1954) 924–933.

[36] J. C. Dechaux, L. Delfosse, The negative temperature coefficient in the C_2 to C_{13} hydrocarbon oxidation. I. Morphological results, Combust. Flame 34 (1979) 161–168.

[37] D. T. A. Townend, E. A. C. Chamberlain, The influence of pressure on the spontaneous ignition of inflammable gas-air mixtures iv - methane-, ethane-, and propane-air mixtures, Proc. R. Soc. A 154 (1936) 95–112.

[38] G. P. Kane, E. A. C. Chamberlain, D. T. A. Townend, The spontaneous ignition under pressure of the simpler aliphatic hydrocarbons, alcohols, and aldehydes, Proc. R. Soc. A (Lond.) 160 (1937) 436–443.

[39] N. M. Chirkov, S. G. Entelis, J. Phys. Chem. U.S.S.R. 22 (1948) 930.

[40] J. Zador, C. A. Taatjes, R. X. Fernandes, Kinetics of elementary reactions in low-temperature autoignition chemistry, Prog. Energy Combust. Sci. 37 (2011) 371–421.

[41] C. Y. Sheng, J. W. Bozzelli, A. M. Dean, A. Y. Chang, Detailed kinetics and thermochemistry of $C_2H_5 + O_2$: Reaction kinetics of the chemically-activated and stabilized CH_3CH_2OO adduct, J. Phys. Chem. A 106 (2002) 7276–7293.

[42] A. C. Davis, J. S. Francisco, Ab initio study of hydrogen migration in 1-alkylperoxy radicals, J. Phys. Chem. A 114 (2010) 11492–11505.

[43] S. Sharma, S. Raman, W. H. Green, Intramolecular hydrogen migration in alkylperoxy and hydroperoxyalkylperoxy radicals: Accurate treatment of hindered rotors, J. Phys. Chem. A 114 (2010) 5689–5701.

[44] S. Grimme, Semiempirical hybrid density functional with perturbative second-order correlation, J. Chem. Phys. 124 (2006) 34108.

[45] S. Grimme, J. Antony, S. Ehrlich, H. Krieg, A consistent and accurate ab initio parametrization of density functional dispersion correction (DFT-D) for the 94 elements H-Pu, J. Chem. Phys. 132 (2010) 154104.

[46] H.-J. Werner, P. J. Knowles, G. Knizia, F. R. Manby, M. Schutz, P. Celani, T. Korona, R. Lindh, A. Mitrushenkov, G. Rauhut, K. R. Shamasundar, T. B. Adler, R. D. Amos, A., Bernhardsson, A. Berning, D. L. Cooper, M. J. O. Deegan, A. J. Dobbyn, F. Eckert, E. Goll, C. Hampel, A. Hesselmann, G. Hetzer, T. Hrenar, G. Jansen, C. Koppl, Y. Liu, A. W. Lloyd, R. A. Mata, A. J. May, S. J. McNicholas, W. Meyer, M. E. Mura, A. Nicklass, D. P. ONeill, P. Palmieri, D. Peng, K. Pfluger, R. Pitzer, M. Reiher, T. Shiozaki, H. Stoll, A. J. Stone, R. Tarroni, T. Thorsteinsson, M. Wang, MOLPRO, version 2012.1, a package of ab initio programs, 2012. URL: `http://www.molpro.net`.

[47] Z. Rolik, L. Szegedy, I. Ladjánszki, B. Ladóczki, M. Kállay, An efficient linear-scaling CCSD (T) method based on local natural orbitals, J. Chem. Phys. 139 (2013) 94105.

[48] J. Stanton, J. Gauss, M. Harding, P. Szalay, A. Auer, R. Bartlett, U. Benedikt, C. Berger, D. Bernholdt, Y. Bomble, L. Cheng, O. Christiansen, M. Heckert, O. Heun, C. Huber, T.-C. Jagau, D. Jonsson, J. Jusélius, K. Klein, W. Lauderdale, F. Lipparini, D. Matthews, T. Metzroth, L. Mück, D. Ó. Neill, D. Price, E. Prochnow, C. Puzzarini, K. Ruud, F. Schiffmann, W. Schwalbach, C. Simmons, S. Stopkowicz, A. Tajti, J. Vázquez, F. Wang, J. Watts, J. Almlöf, P. Taylor, P. Taylor, T. Helgaker, H. A. Jensen, P. Jrgensen, J. Olsen, A. V. Mitin, C. van Wüllen, CFOUR, coupled-cluster techniques for computational chemistry, a quantum-chemical program package (2015). For the current version, see http://www.cfour.de.

[49] M. J. Frisch, G. W. Trucks, H. B. Schlegel, G. E. Scuseria, M. A. Robb, J. R. Cheeseman, G. Scalmani, V. Barone, B. Mennucci, G. A. Petersson, H. Nakatsuji,

M. Caricato, X. Li, H. P. Hratchian, A. F. Izmaylov, J. Bloino, G. Zheng, J. L. Sonnenberg, M. Hada, M. Ehara, K. Toyota, R. Fukuda, J. Hasegawa, M. Ishida, T. Nakajima, Y. Honda, O. Kitao, H. Nakai, T. Vreven, J. A. Montgomery Jr., J. E. Peralta, F. Ogliaro, M. Bearpark, J. J. Heyd, E. Brothers, K. N. Kudin, V. N. Staroverov, R. Kobayashi, J. Normand, K. Raghavachari, A. Rendell, J. C. Burant, S. S. Iyengar, J. Tomasi, M. Cossi, N. Rega, J. M. Millam, M. Klene, J. E. Knox, J. B. Cross, V. Bakken, C. Adamo, J. Jaramillo, R. Gomperts, R. E. Stratmann, O. Yazyev, A. J. Austin, R. Cammi, C. Pomelli, J. W. Ochterski, R. L. Martin, K. Morokuma, V. G. Zakrzewski, G. A. Voth, P. Salvador, J. J. Dannenberg, S. Dapprich, A. D. Daniels, O. Farkas, J. B. Foresman, J. V. Ortiz, J. Cioslowski, D. J. Fox, Gaussian 09 Revision A.1, 2009.

[50] Y. Georgievskii, J. A. Miller, M. P. Burke, S. J. Klippenstein, Reformulation and solution of the master equation for multiple-well chemical reactions, J. Phys. Chem. A 117 (2013) 12146–12154.

[51] A. W. Jasper, J. A. Miller, Lennard–Jones parameters for combustion and chemical kinetics modeling from full-dimensional intermolecular potentials, Combust. Flame 161 (2014) 101–110.

[52] A. W. Jasper, 2016. Private communication.

[53] J. A. Miller, S. J. Klippenstein, S. H. Robertson, A theoretical analysis of the reaction between ethyl and molecular oxygen, Proc. Combust. Inst. 28 (2000) 1479–1486.

[54] J. A. Miller, M. J. Pilling, J. Troe, Unravelling combustion mechanisms through a quantitative understanding of elementary reactions, Proc. Combust. Inst. 30 (2005) 43–88.

[55] S. J. Klippenstein, Y. Georgievskii, L. B. Harding, Predictive theory for the combination kinetics of two alkyl radicals, Phys. Chem. Chem. Phys. 8 (2006) 1133–1147.

[56] R. Sivaramakrishnan, J. V. Michael, B. Ruscic, High-temperature rate constants for H/D + C_2H_6 and C_3H_8, Int. J. Chem. Kinet. 44 (2012) 194–205.

[57] D. L. Baulch, C. T. Bowman, C. J. Cobos, R. A. Cox, T. Just, J. A. Kerr, M. J. Pilling, D. Stocker, J. Troe, W. Tsang, R. W. Walker, J. Warnatz, Evaluated kinetic data for combustion modeling: Supplement II, J. Phys. Chem. Ref. Data 34 (2005) 757–1397.

[58] L. N. Krasnoperov, J. V. Michael, Shock tube studies using a novel multipass absorption cell: Rate constant results for OH + H_2 and OH + C_2H_6, J. Phys. Chem. A 108 (2004) 5643–5648.

[59] A. S. Sharipov, A. M. Starik, Theoretical study of the reaction of ethane with oxygen molecules in the ground triplet and singlet delta states, J. Phys. Chem. A 116 (2012) 8444–8454.

[60] S. L. Peukert, N. J. Labbe, R. Sivaramakrishnan, J. V. Michael, Direct measurements of rate constants for the reactions of CH_3 radicals with C_2H_6, C_2H_4, and C_2H_2 at high temperatures, J. Phys. Chem. A 117 (2013) 10228–10238.

[61] J. A. Miller, S. J. Klippenstein, The H + C_2H_2 (+M) = C_2H_3 (+M) and H + C_2H_2 (+M) = C_2H_5 (+M) reactions: Electronic structure, variational transition-state theory, and solutions to a two-dimensional master equation, Phys. Chem. Chem. Phys. 6 (2004) 1192–1202.

[62] N. J. Labbe, R. Sivaramakrishnan, S. J. Klippenstein, The role of radical + fuel-radical well-skipping reactions in ethanol and methylformate low-pressure flames, Proc. Combust. Inst. 35 (2015) 447–455.

[63] A. Noell, L. Alconcel, D. Robichaud, M. Okumura, S. Sander, Near-infrared kinetic spectroscopy of the ho2 and c2h5o2 self-reactions and cross reactions, J. Phys. Chem. A 114 (2010) 6983–6995.

[64] D. Chen, H. Jin, Z. Wang, L. Zhang, F. Qi, Unimolecular decomposition of ethyl hydroperoxide: Ab initio/Rice-Ramsperger-Kassel-Marcus theoretical prediction of rate constants, J. Phys. Chem. A 115 (2011) 602–611.

[65] E. E. Dames, Master equation modeling of the unimolecular decompositions of alpha-hydroxyethyl (CH_3CHOH) and ethoxy (CH_3CH_2O) radicals, Int. J. Chem. Kinet. 46 (2014) 176–188.

[66] N. J. Labbe, R. Sivaramakrishnan, C. F. Goldsmith, Y. Georgievskii, J. A. Miller, S. J. Klippenstein, Weakly bound free radicals in combustion: prompt dissociation of formyl radicals and its effect on laminar flame speeds, J. Phys. Chem. Lett. 7 (2016) 85–89.

[67] M. Sangwan, C. Yan, E. N. Chesnokov, L. N. Krasnoperov, Reaction CH_3+ CH_3 $\rightarrow$ C_2H_6 studied over the 292–714 K temperature and 1–100 bar pressure ranges, J. Phys. Chem. A 119 (2015) 7847–7857.

[68] R. R. Baldwin, C. E. Dean, M. R. Honeyman, R. W. Walker, Arrhenius parameters for the reaction HO_2 +C_2H_6 $\rightarrow$ C_2H_5+H_2O_2 over the temperature range 400–500 C, J. Chem. Soc., Faraday Trans. 1 82 (1986) 89–102.

[69] D. D. Y. Zhou, K. Han, P. Zhang, L. B. Harding, M. J. Davis, R. T. Skodje, Theoretical determination of the rate coefficient for the HO_2 + HO_2 = H_2O_2 + O_2 reaction: Adiabatic treatment of anharmonic torsional effects, J. Phys. Chem. A 116 (2012) 2089–2100.

[70] H.-H. Carstensen, A. M. Dean, O. Deutschmann, Rate constants for the H abstraction from alkanes (R–H) by $R'O_2$ radicals: A systematic study on the impact of R and R′, Proc. Combust. Inst. 31 (2007) 149–157.

[71] J. Aguilera-Iparraguirre, H. J. Curran, W. Klopper, J. M. Simmie, Accurate Benchmark Calculation of the Reaction Barrier Height for Hydrogen Abstraction by the Hydroperoxyl Radical from Methane. Implications for C_nH_{2n+2} where n = 2 $\rightarrow$ 4, J. Phys. Chem. A 112 (2008) 7047–7054.

[72] J. P. Senosiain, S. J. Klippenstein, J. A. Miller, Reaction of ethylene with hydroxyl radicals: A theoretical study, J. Phys. Chem. A 110 (2006) 6960–6970.

[73] S. S. Vasu, Z. Hong, D. F. Davidson, R. K. Hanson, D. M. Golden, Shock tube/laser absorption measurements of the reaction rates of OH with ethylene and propene, J. Phys. Chem. A 114 (2010) 11529–11537.

[74] Reaction Design, CHEMKIN-PRO 15131, 2013.

[75] S. Gersen, N. B. Anikin, A. V. Mokhov, H. B. Levinsky, Ignition properties of methane/hydrogen mixtures in a rapid compression machine, Int. J. Hydrog. Energy 33 (2008) 1957–1964.

[76] D. Lee, S. Hochgreb, Rapid compression machines: Heat transfer and suppression of corner vortex, Combust. Flame 114 (1998) 531–545.

[77] P. Park, Rapid compression measurements of ignition delays for primary reference fuels, PhD thesis - MIT, 1990.

[78] D. Lee, Autoignition measurements and modelling in a rapid compression machine, PhD thesis - MIT, 1997.

[79] G. Mittal, C.-J. Sung, R. A. Yetter, Autoignition of H_2/CO at elevated pressures in a rapid compression machine, Int. J. Chem. Kinet. 38 (2006) 516–529.

[80] S. Tanaka, F. Ayala, J. C. Keck, A reduced chemical kinetic model for HCCI combustion of primary reference fuels in a rapid compression machine, Combust. Flame 133 (2003) 467–481.

[81] A. E. Lutz, R. J. Kee, J. A. Miller, SENKIN: A FORTRAN program for predicting homogeneous gas phase chemical kinetics with sensitivity analysis, Technical Report MS-9051, Sandia National Laboratories, Livermore, 1988.

[82] R. J. Kee, F. M. Rupley, J. A. Miller, Chemkin-II: A Fortran chemical kinetics package for the analysis of gas-phase chemical kinetics, Technical Report, Sandia National Labs., Livermore, CA (USA), 1989.

[83] L. Pan, Y. Zhang, J. Zhang, Z. Tian, Z. Huang, Shock tube and kinetic study of $C_2H_6/H_2/O_2$/Ar mixtures at elevated pressures, Int. J. Hydrog. Energy 39 (2014) 6024–6033.

[84] E. Hu, Y. Chen, Z. Zhang, X. Li, Y. Cheng, Z. Huang, Experimental study on ethane ignition delay times and evaluation of chemical kinetic models, Energy Fuels 29 (2015) 4557–4566.

[85] C. M. Vagelopoulos, F. N. Egolfopoulos, Direct experimental determination of laminar flame speeds, Symp. (Int.) Combust., [Proc.] 27 (1998) 513–519.

[86] A. A. Konnov, I. V. Dyakov, J. De Ruyck, Measurement of adiabatic burning velocity in ethane-oxygen-nitrogen and in ethane-oxygen-argon mixtures, Exp. Therm. Fluid Sci. 27 (2003) 379–384.

[87] G. Jomaas, X. L. Zheng, D. L. Zhu, C. K. Law, Experimental determination of counterflow ignition temperatures and laminar flame speeds of C_2-C_3 hydrocarbons at atmospheric and elevated pressures, Proc. Combust. Inst. 30 (2005) 193–200.

[88] I. V. Dyakov, J. De Ruyck, A. A. Konnov, Probe sampling measurements and modeling of nitric oxide formation in ethane+air flames, Fuel 86 (2007) 98–105.

[89] W. Lowry, J. de Vries, M. Krejci, E. Petersen, Z. Serinyel, W. Metcalfe, H. Curran, G. Bourque, Laminar flame speed measurements and modeling of pure alkanes and alkane blends at elevated pressures, J. Eng. Gas Turbines Power 133 (2011) 91501.

[90] M. Goswami, Laminar burning velocities at elevated pressures using the heat flux method, Ph.D. thesis, Technische Universiteit Eindhoven, 2014.

[91] C. K. Law, F. Wu, F. N. Egolfopoulos, V. Gururajan, H. Wang, On the rational interpretation of data on laminar flame speeds and ignition delay times, Combust. Sci. Technol. 187 (2015) 27–36.

[92] F. N. Egolfopoulos, D. L. Zhu, C. K. Law, Experimental and numerical determination of laminar flame speeds: Mixtures of C2-hydrocarbons with oxygen and nitrogen, Symp. (Int.) Combust., [Proc.] 23 (1991) 471–478.

[93] M. I. Hassan, K. T. Aung, O. C. Kwon, G. M. Faeth, Properties of laminar premixed hydrocarbon/air flames at various pressures, J. Propul. Power 14 (1998) 479–488.

[94] K. Kumar, G. Mittal, C.-J. Sung, C. K. Law, An experimental investigation of ethylene/O_2/diluent mixtures: Laminar flame speeds with preheat and ignition delays at high pressures, Combust. Flame 153 (2008) 343–354.

[95] E. Rokni, A. Moghaddas, O. Askari, H. Metghalchi, Measurement of laminar burning speeds and investigation of flame stability of acetylene C_2H_2/air mixtures, J. Energy Resour. Technol. 137 (2015) 012204.

[96] O. Park, P. S. Veloo, N. Liu, F. N. Egolfopoulos, Combustion characteristics of alternative gaseous fuels, Proc. Combust. Inst. 33 (2011) 887–894.